Symbolic Coding for Noninvertible Systems: Uniform Approximation and Numerical Computation

Wolf-Jürgen Beyn* Thorsten Hüls* Andre Schenke*

Department of Mathematics, Bielefeld University

POB 100131, 33501 Bielefeld, Germany

`beyn@math.uni-bielefeld.de`

`huels@math.uni-bielefeld.de`

`aschenke@math.uni-bielefeld.de`

March 22, 2016

Abstract

It is well known that the Homoclinic Theorem, which conjugates a map near a transversal homoclinic orbit to a Bernoulli subshift, extends from invertible to specific noninvertible dynamical systems. In this paper, we provide a unifying approach, which combines such a result with a fully discrete analog of the conjugacy for finite but sufficiently long orbit segments. The underlying idea is to solve appropriate discrete boundary value problems in both cases, and to use the theory of exponential dichotomies for controlling the errors. This leads to a numerical approach which allows to compute the conjugacy to any prescribed accuracy. The method is demonstrated for several examples where invertibility of the map fails in different ways.

Keywords: Noninvertible dynamical systems, homoclinic orbits, symbolic coding, numerical computation

AMS Subject Classification: 65P20, 37B10, 65Q10, 37C29

1   Introduction

Quite a few fundamental theorems on invertible dynamical systems have found suitable analogs in the theory of noninvertible systems. In this paper we reconsider corresponding generalizations of the well-known Homoclinic Theorem (see Smale [40] and Šil′nikov [39]) on the symbolic coding of maximal invariant sets near a transversal homoclinic point. Our main goal is to set up and analyze a numerical approach that allows to compute all symbolically coded orbits near a homoclinic orbit of a noninvertible system up to a prescribed tolerance.

The motivation for studying noninvertible maps comes from different sources. One major source are maps in infinite-dimensional Banach spaces which arise as flow maps or Poincaré maps of partial differential equations and delay differential equations. We mention the work of Hale and Lin [12] and, in particular, the ensuing work of Steinlein and Walther [41], [42] which gives a rather complete picture of shadowing and symbolic coding near homoclinics in the noninvertible case. In the work of Kalkbrenner [22] (see also the survey in [2]), the closely related notion of exponential dichotomy was generalized to noninvertible and nonautonomous systems and then applied to characterize symbolic coding near homoclinics. The proposed notion of a 'regular exponential dichotomy' agrees with the earlier definition by Henry [14, Ch. 7], and the proof of symbolic coding employs Palmer's method for proving the Homoclinic Theorem for invertible systems [31], [32]. We also mention modern results on so called generalized Hénon maps from [9], [11] as well as the work of Sander [35] which generalizes the notions of hyperbolicity and homoclinic tangles from nonlinear maps to nonlinear relations.

A second source of noninvertibility are reduced models of higher dimensional dynamical systems which allow to study chaotic dynamics in low dimensions. A characteristic example, which will also be treated in this paper, is a noninvertible two-dimensional model for 'wild chaos', derived in [5] from a 5-dimensional invertible system and investigated extensively in [15], [16].

In the following, we describe in more detail the contents of this paper by putting some emphasis on our computational approach. In particular, we treat finite orbit segments approximating the symbolic coding of noninvertible maps, and we provide an alternative road to proving the Homoclinic Theorem in the biinfinite case.

Since we aim at numerical computations we consider a finite-dimensional smooth map $f : \mathbb{R}^d \to \mathbb{R}^d$ and its induced dynamical system

$$x_{n+1} = f(x_n), \quad x_n \in \mathbb{R}^d, \quad n \in \mathbb{Z}.$$

Moreover, we assume that we are given a fixed point

$$\xi = f(\xi) \in \mathbb{R}^d$$

and an associated nontrivial homoclinic orbit $\bar{x}_\mathbb{Z} = (\bar{x}_n)_{n \in \mathbb{Z}}$, i.e.

$$\bar{x}_{n+1} = f(\bar{x}_n), \quad n \in \mathbb{Z}, \quad \lim_{n \to \pm\infty} \bar{x}_n = \xi, \quad \bar{x}_n \neq \xi \text{ for some } n \in \mathbb{Z}.$$

Our basic assumption states that the variational equation

$$u_{n+1} = Df(\bar{x}_n)u_n, \quad n \in \mathbb{Z} \tag{1}$$

has an exponential dichotomy on $\mathbb{Z}$ according to Definition 18. We emphasize that this definition does not assume $Df(\bar{x}_n)$ to be invertible, but we refrain from using the term 'regular dichotomy' from [22] for this situation. Also note that an exponential dichotomy in this sense implies hyperbolicity of the set

$$\mathcal{H} = \{\xi\} \cup \{\bar{x}_n : n \in \mathbb{Z}\} \tag{2}$$

as defined in [42, Def. 1.1] (in fact, both properties are equivalent in the finite-dimensional case).

In the invertible, finite-dimensional case, the condition that (1) has an exponential dichotomy on $\mathbb{Z}$ is equivalent to the homoclinic orbit lying on the intersection of the stable and unstable manifold to the fixed point and this intersection being transversal, c.f. [32, Proposition 5.6].

If the intersection is not transversal but tangential, the resulting orbit is called a homoclinic tangency. Homoclinic tangencies show quite intricate dynamical behavior, c.f. [6], [10], [29], [35] and references therein.

For any bounded open set $\mathcal{O} \subset \mathbb{R}^d$ we define the set of orbits remaining in $\mathcal{O}$ by

$$\mathrm{Orb}(\mathcal{O}) = \{x_{\mathbb{Z}} \in (\mathbb{R}^d)^{\mathbb{Z}} : x_n \in \mathcal{O}, \ x_{n+1} = f(x_n) \text{ for all } n \in \mathbb{Z}\}. \tag{3}$$

This set is closed in $\mathcal{O}^{\mathbb{Z}}$ when endowed with the product topology, and it is invariant under the orbit shift induced by f,

$$\mathcal{F}(x_{\mathbb{Z}}) := (f(x_n))_{n \in \mathbb{Z}}. \tag{4}$$

It is shown in [42] that there exists a neighborhood $\mathcal{O}$ of $\mathcal{H}$, a number $N \in \mathbb{N}$ and a homeomorphism h which conjugates $\mathcal{F} : \mathrm{Orb}(\mathcal{O}) \to \mathrm{Orb}(\mathcal{O})$ to a subshift $(\Sigma^{\mathbb{Z}}_{A(N)}, \sigma)$:

$$
\begin{array}{ccc}
\Sigma^{\mathbb{Z}}_{A(N)} & \xrightarrow{\ \sigma\ } & \Sigma^{\mathbb{Z}}_{A(N)} \\
{\scriptstyle h}\downarrow & & \downarrow{\scriptstyle h} \qquad \mathcal{F} \circ h = h \circ \sigma. \\
\mathrm{Orb}(\mathcal{O}) & \xrightarrow[\ \mathcal{F}\ ]{} & \mathrm{Orb}(\mathcal{O})
\end{array}
\tag{5}
$$

Here, $S_N^{\mathbb{Z}} := \{0, \cdots, N-1\}^{\mathbb{Z}}$ is the space of symbolic sequences on N symbols endowed with the product topology, σ denotes the Bernoulli shift and $\Sigma^{\mathbb{Z}}_{A(N)} \subset S_N^{\mathbb{Z}}$ is the topological Markov chain

$$\Sigma^{\mathbb{Z}}_{A(N)} = \{s \in S_N^{\mathbb{Z}} : A(N)_{s_j, s_{j+1}} = 1, \ j \in \mathbb{Z}\}$$

defined by the matrix

$$
A(N) = \begin{pmatrix}
1 & 1 & 0 & \cdots & 0 \\
0 & 0 & 1 & \ddots & 0 \\
\vdots & \vdots & \ddots & \ddots & 0 \\
0 & 0 & & \ddots & 1 \\
1 & 0 & \cdots & \cdots & 0
\end{pmatrix} \in \{0,1\}^{N,N}.
$$

As in [42] it is not difficult to retrieve the classical Homoclinic Theorem for the invertible case from this result by adding another conjugacy to the diagram in (5) that assigns to any orbit $x_{\mathbb{Z}} \in \mathrm{Orb}(\mathcal{O})$ a single point such as x_0.

In our approach we consider also the finite time case $S_N^J = \{0, \ldots, N-1\}^J$, where $J = [n_-, n_+] = \{n \in \mathbb{Z} : n_- \le n \le n_+\}$, $-\infty < n_- < n_+ < \infty$. Setting $\tilde{J} = [n_-, n_+ - 1]$, we then define $\Sigma^J_{A(n)}$ by

$$\Sigma^J_{A(N)} = \{s \in S_N^J : s_{n_-} = s_{n_+} = 0, \ A(N)_{s_j, s_{j+1}} = 1, j \in \tilde{J}\}. \tag{6}$$

Finite orbits are determined as solutions of boundary value problems

$$x_{n+1} = f(x_n), \ n = n_-, \ldots, n_+ - 1, \quad b(x_{n_-}, x_{n_+}) = 0 \qquad (7)$$

with boundary operators $b : \mathbb{R}^d \times \mathbb{R}^d \to \mathbb{R}^d$ satisfying a nondegeneracy condition, see Section 4. With the set of finite orbits defined by

$$\mathrm{Orb}(J, \mathcal{O}) := \{x_J \in \mathcal{O}^J : x_J = (x_n)_{n \in J} \text{ solves } (7)\},$$

our finite time analog of the diagram (5) takes the form

$$
\begin{array}{ccc}
\Sigma_{A(N)}^{J} & \xrightarrow{\ \sigma_J\ } & \Sigma_{A(N)}^{J-1} \\
{\scriptstyle h_J}\downarrow & & \downarrow{\scriptstyle h_{J-1}} \\
\mathrm{Orb}(J, \mathcal{O}) & \xrightarrow[\ \mathcal{F}_J\ ]{} & \mathrm{Orb}(J-1, \mathcal{O})
\end{array}
\qquad (8)
$$

In this diagram we use the shifted interval $J - 1 = [n_- - 1, n_+ - 1]$ and the finite Bernoulli shift

$$
\begin{aligned}
\sigma_J : \Sigma_{A(N)}^{J} &\to \Sigma_{A(N)}^{J-1}, \\
a_J &\mapsto b_{J-1}, \quad \text{with } b_n = a_{n+1}, \text{ for } n \in J - 1.
\end{aligned}
\qquad (9)
$$

Note that due to the shift of interval from J to $J - 1$, the endpoint condition in (6) is automatically satisfied. Furthermore the map $\mathcal{F}_J$ in (8) is defined by

$$
\begin{aligned}
\mathcal{F}_J : \mathcal{O}^J &\to \mathcal{O}^{J-1}, \\
x_J &\mapsto y_{J-1}, \quad \text{with} \quad y_n = \begin{cases} x_{n_-}, & \text{for } n = n_- - 1, \\ f(x_n), & \text{for } n \in \tilde{J}. \end{cases}
\end{aligned}
\qquad (10)
$$

This operator satisfies $\mathcal{F}_J : \mathrm{Orb}(J, \mathcal{O}) \to \mathrm{Orb}(J-1, \mathcal{O})$ since it preserves the boundary condition. With these settings we obtain a complete finite time analog of the Homoclinic Theorem in Theorem 14.

In the following, we discuss the further results of this paper. In Section 2.1, we consider systems, for which several homoclinic orbits exist, connecting to the same fixed point. We indicate how the finite time conjugacy from above and its numerical computation can be generalized. In Section 2.2 we turn the theoretical approach into a numerical algorithm. For a given symbolic sequence $s_J \in \Sigma_{A(N)}^{J}$, we compute the orbit segment $h_J(s_J)$ in $\mathrm{Orb}(J, \mathcal{O})$ from the solution of an appropriate boundary value problem. Our approximation theory shows that these boundary value problems are well-conditioned in the neighborhood of suitable pseudo-orbits despite the fact that the map f is noninvertible. This will be demonstrated for a series of examples in Section 6.

The theoretical part of our paper is the subject of Sections 3 and 4. The starting point is the Roughness Theorem for exponential dichotomies in the noninvertible case (see [22], [14] and Theorem 20 in the Appendix). We indicate an alternative proof by a direct perturbation argument for the Green's function in an exponentially weighted space. The argument follows an idea of Sandstede [36], [37] for flows, which has been transferred to invertible mappings in the work of Kleinkauf [23], [25]. Then we consider

4

pseudo-orbits obtained by piecing together the original homoclinic orbit according to the coding sequence $s_{\mathbb{Z}} \in \Sigma_{A(N)}^{\mathbb{Z}}$. In Theorem 4 we show that the variational equations from a suitable neighborhood of the pseudo-orbits have an exponential dichotomy with data independent of the coding. This result has a complete analog for finite orbit segments, see Theorem 6.

With these preparations we prove solvability of discrete boundary value problems on both finite and infinite time intervals, see Theorem 7. For the infinite case this result replaces the Shadowing Lemma for noninvertible maps from [22] (see the monographs [34], [30] for invertible maps). For the solutions of finite boundary value problems we show error estimates which decay towards the interior and which are uniform with respect to the coding sequence (Corollary 9).

As a consequence, in Theorem 10 we prove convergence of solution sets of finite orbits to those of infinite orbits. Convergence holds with respect to the Hausdorff distance

$$\text{dist}_{\text{H}}(X, Y) = \max \left(\sup_{x \in X} \inf_{y \in Y} \text{dist}(x, y), \sup_{y \in Y} \inf_{x \in X} \text{dist}(x, y) \right), \tag{11}$$

where the distance of finite segments is defined by

$$\text{dist}(x_J, y_J) = \sum_{n=n_-}^{n_+} 2^{-|n|} |x_n - y_n|. \tag{12}$$

Note that this metric converges as $n_{\pm} \to \pm\infty$ to the metric

$$\text{dist}(x_{\mathbb{Z}}, y_{\mathbb{Z}}) = \sum_{n \in \mathbb{Z}} 2^{-|n|} |x_n - y_n|, \quad x_{\mathbb{Z}}, y_{\mathbb{Z}} \in \mathcal{O}^{\mathbb{Z}},$$

which defines the product topology on $\mathcal{O}^{\mathbb{Z}}$. The whole approach extends earlier approximation results for homoclinic tangles in the invertible case [7] and for single connecting orbits in the nonautonomous case [19].

In Section 5 we show how the Homoclinic Theorem for the noninvertible case derives naturally from these results. A crucial step here is to construct an open neighborhood $\mathcal{O}$ such that the orbit set $\text{Orb}(\mathcal{O})$ from (3) agrees with the set of orbits coded by symbolic sequences, see Theorem 12.

In Section 6 numerical computations are shown for the classical (invertible) Hénon example, a three-dimensional Hénon map and for a modified Hénon example where the dynamics collapses into a line and a snap-back repeller occurs (cf. [26]). Then we use our approach to investigate chaotic features created by homoclinic orbits in the noninvertible model of 'wild chaos' from [5], [15] and in a recent model of asset pricing from [8].

2   Numerical computation of the maximal invariant set

We propose an algorithm for the approximation of points from the maximal invariant set

$$\mathcal{O}_c := \{x_0 : x_{\mathbb{Z}} \in \text{Orb}(\mathcal{O})\}. \tag{13}$$

Note that $\mathcal{O}_c$ typically is a Cantor set on which f-dynamics are semi-conjugate to $\mathcal{F}$-dynamics on $\mathrm{Orb}(\mathcal{O})$, i.e.

$$
\begin{array}{ccc}
\mathrm{Orb}(\mathcal{O}) & \xrightarrow{\ \mathcal{F}\ } & \mathrm{Orb}(\mathcal{O}) \\
{\scriptstyle r}\big\downarrow & & \big\downarrow{\scriptstyle r} \\
\mathcal{O}_c & \xrightarrow{\ \ f\ \ } & \mathcal{O}_c
\end{array}
\qquad f \circ r = r \circ \mathcal{F},
$$

where r is sujective. Indeed, if f is invertible, then r turns out to be a homeomorphism, resulting in a conjugacy of f-dynamics on $\mathcal{O}_c$ to the shift on $\Sigma_{A(N)}^{\mathbb{Z}}$.

Further note that stable and unstable manifolds of the fixed point ξ intersect at each point $x \in \mathcal{O}_c$ transversally, assuming the hyperbolicity assumptions, introduced in Section 3. Finding intersection points of these two manifolds is rather involved. Instead, we calculate points in $\mathcal{O}_c$ via homoclinic orbits, that we approximate numerically by solving boundary value problems. Manifolds are plotted only for illustrating the output of this ansatz.

Before the algorithm is introduced in detail, we extend to a slightly more general setup.

2.1 Combining several homoclinic orbits

If only one primary homoclinic orbit is considered, one misses several points of intersection of stable and unstable manifolds, see the left panel in Figure 5 for an illustration. Thus, we generalize immediately to multi-humped orbits that are constructed from ℓ different primary homoclinic orbits x_J^i, $i = 1, \ldots, \ell$ w.r.t. the same fixed point ξ. It turns out that there exists for each $i \in \{1, \ldots, \ell\}$ a number N_i and corresponding neighborhoods that allow the coding of multi-humped orbits with $L = 1 + \sum_{i=1}^{\ell} N_i$ symbols. For details, we refer to Theorems 11 and 14. More precisely, we find a homeomorphism between multi-humped orbits in these neighborhoods and sequences of L symbols $s_{\mathbb{Z}} \in \Sigma_{A(N_1, \ldots, N_\ell)}$, where

$$
A(N_1, \ldots, N_\ell) = \begin{pmatrix}
1 & 1 & & 1 & \cdots & \cdots & 1 \\
& & I_1 & & & & \\
1 & & & & & & \\
& & & & I_2 & & \\
1 & & & & & & \\
\vdots & & & & & \ddots & \\
\vdots & & & & & & \ddots \\
& & & & & & I_\ell \\
1 & & & & & &
\end{pmatrix}
$$

and I_i denotes the identity in $\mathbb{R}^{N_i-1, N_i-1}$, $i = 1, \ldots, \ell$. In this section, we do not introduce different notions for finite and infinite time intervals. While the case $J = \mathbb{Z}$ is presented here, the finite time case requires suitable boundary conditions, see (6).

We further simplify notions by coding this Markov chain with $\ell+1$ symbols $s_{\mathbb{Z}} \in \Sigma_{A(1^\ell)}$

$$A(1^\ell) = \begin{pmatrix} 1 & 1 & \cdots & 1 \\ 1 & & & \\ \vdots & & & \\ 1 & & & \end{pmatrix} \in \{0,1\}^{\ell+1,\ell+1}$$

and by an extended set

$$\Sigma^*_{A(1^\ell)} = \{(s_{\mathbb{Z}}, n) : s_{\mathbb{Z}} \in \Sigma_{A(1^\ell)}, n \in \{1, \ldots, N_{s_0}\}\}.$$

The purpose of the second component n is to serve as a pointer for the current position. This enables us to establish a one to one connection between $\Sigma_{A(N_1,\ldots,N_\ell)}$ and $\Sigma^*_{A(1^\ell)}$.

For $(s_{\mathbb{Z}}, k) \in \Sigma^*_{A(1^\ell)}$, we define $g : \Sigma^*_{A(1^\ell)} \to \Sigma_{A(N_1,\ldots,N_\ell)}$:

$$g(s_{\mathbb{Z}}, k) := (\cdots, a(s_{-1}), a(s_0), a(s_1), \ldots) \tag{14}$$

where $N_0 := 1$ and

$$a(s_i) := \left(\sum_{j=0}^{s_{i-1}} N_j, \ldots, -1 + \sum_{j=0}^{s_i} N_j \right), \quad i \in \mathbb{Z}, \quad \text{such that} \quad g(s_{\mathbb{Z}}, k)_0 = a(s_0)_k.$$

Denote by σ_L and σ_ℓ the Bernoulli shift on $\Sigma_{A(N_1,\ldots,N_\ell)}$ and on $\Sigma_{A(1^\ell)}$, respectively and define

$$\sigma^*_\ell(s_{\mathbb{Z}}, i) = \begin{cases} (\sigma_\ell(s_{\mathbb{Z}}), 1), & \text{if } i = N_{s_0}, \\ (s_{\mathbb{Z}}, i+1), & \text{otherwise.} \end{cases}$$

A direct computation shows that the diagram

$$\begin{array}{ccc} \Sigma_{A(N_1,\ldots,N_\ell)} & \xrightarrow{\sigma_L} & \Sigma_{A(N_1,\ldots,N_\ell)} \\ \Big\uparrow{\scriptstyle g} & & \Big\uparrow{\scriptstyle g} \\ \Sigma^*_{A(1^\ell)} & \xrightarrow[\sigma^*_\ell]{} & \Sigma^*_{A(1^\ell)} \end{array}$$

commutes. Consequently, we obtain a conjugacy between this shift-dynamics and the $\mathcal{F}$-dynamics on $\mathrm{Orb}(\mathcal{O})$, where $\mathcal{O}$ is a sufficiently small neighborhood of the ℓ primary homoclinic orbits.

2.2 The algorithm

We introduce our numerical method for computing an approximation of the maximal invariant set $\mathcal{O}_c$ close to a given point of a homoclinic orbit. Here, we assume that the map $f \in \mathbb{C}^1(\mathbb{R}^d \times \mathbb{R}, \mathbb{R}^d)$ depends on a one-dimensional parameter p and we aim at an approximation for the fixed parameter value $\bar{p}$. We abbreviate $f(\cdot)$ for $f(\cdot, \bar{p})$.

The algorithm works along the following steps.

(Ia) Compute a first homoclinic orbit segment x^1_J on a finite interval $J = [j_-, j_+]$ by solving the boundary value problem (7) using Newton's method. For a discussion of appropriate boundary conditions, we refer to Section 4.1.

(Ib) Calculate a curve of homoclinic $f(\cdot, p)$-orbits w.r.t. the parameter p by applying numerical continuation techniques, see [1, Algorithm 10.2.10]. Detect further homoclinic orbits $x_J^2, \ldots, x_J^\ell$ ($\ell \in \mathbb{N}$) lying on this curve at the parameter value $\bar{p}$.

(II) Choose $k_\pm \in \mathbb{Z}$, $k_- < 0 < k_+$ and consider all sequences $s_{[k_-,k_+]} \in \Sigma_{A(1^\ell)}$ satisfying

$$s_0 = 1, \quad \#\{k_- \leq i \leq -1 : s_i \geq 1\} = 1, \quad \#\{1 \leq i \leq k_+ : s_i \geq 1\} = 1. \qquad (15)$$

We refer to the beginning of this Section for corresponding notions and to Figure 1 for an illustration.

(III) Define the pseudo-orbit w.r.t. the code sequence $(s_{[k_-,k_+]}, j_- + 1) \in \Sigma_{A(1^\ell)}^*$ by replacing the symbol 0 with the fixed point ξ and the symbol i with the orbit segment x_J^i, $i = 1, \ldots, \ell$, respectively.

(IV) Compute a corresponding orbit segment $y_{\hat{J}}$ by applying Newton's method on $\hat{J} := [m_-, m_+]$, $m_- = 2j_- - j_+ + k_-$, $m_+ = 2j_+ - j_- + k_+$ to the boundary value problem

$$\begin{aligned} y_{n+1} &= f(y_n), \quad n = m_-, \ldots, m_+ - 1, \\ 0 &= b(y_{m_-}, y_{m_+}), \end{aligned}$$

starting at the pseudo-orbit from step (III).

(V) Plot the midpoints y_0 of these orbits for all finite code sequences from step (II).

Additionally, we compute approximations of the unstable and stable manifold of the fixed point ξ. For the latter task, we apply a contour algorithm that is introduced in [20] and which applies to a wide class of dynamical systems, including invertible and noninvertible maps.

In Section 6 we demonstrate the performance of the algorithm by applying it to several two and one three-dimensional systems, showing various dynamical features.

Its applicability is formally justified by the following theorem in anticipation of the assumptions **(A1)**-**(A4)** discussed in Section 3 and of condition **(A5)** from Section 4.1.

Theorem 1 *Assume that the exact primary homoclinic orbits $x_{\mathbb{Z}}^1, \ldots, x_{\mathbb{Z}}^\ell$ satisfy the assumptions **(A1)**-**(A4)**, and the boundary operator b satisfies condition **(A5)**. Then there exist constants $C, \beta_s, \beta_u > 0$ such that for all sufficiently large $-j_-$, j_+ the following statement holds true: Fix $k_- < 0 < k_+$ and let $y_{\hat{J}}$ be the solution of the boundary value problem from step (IV). Then there exists an $x_0 \in \mathcal{O}_c$ such that*

$$\|y_0 - x_0\| \leq C(\mathrm{e}^{\beta_s m_-} + \mathrm{e}^{-\beta_u m_+}).$$

As a consequence, approximation errors, occurring in step (V) of the algorithm, are exponentially small.

In the forthcoming sections, we provide the theoretical background for proving Theorem 1 and the Homoclinic Theorem. For a concise presentation, we restrict ourselves to the case of $\ell = 1$ primary homoclinic orbit. After developing this framework, Theorem 1 then directly follows by generalizing Theorem 8 and Corollary 9 in a straightforward manner to the case of different primary orbits.
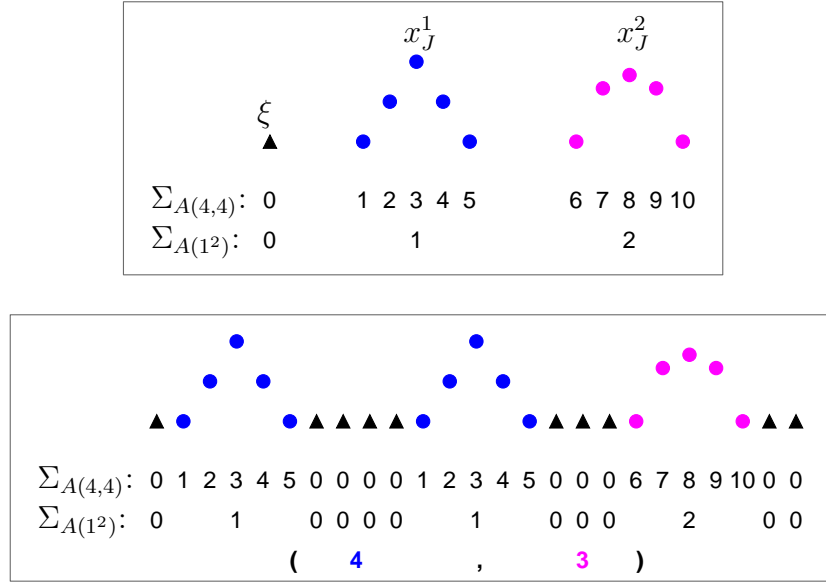
Figure 1: Upper diagram: A sketch of two homoclinic orbit segments $x_J^{1,2}$, $J = [-2, 2]$ and of the fixed point ξ together with their coding in $\Sigma_{A(4,4)}$ and $\Sigma_{A(1^2)}$, respectively. The lower diagram illustrates the construction and coding of multi-humped orbits in case $\pm k_\pm = 6$. The code sequence in the last row – which we formally introduce in Section 6.2 – represents the number of 0-symbols on the left and right side of the center hump. The colors of these two numbers symbolize the type of the neighboring hump.

3 Uniform dichotomies of variational equations

In this section we show that exponential dichotomies along a homoclinic orbit extend in a uniform way to arbitrary orbits obtained by concatenating sufficiently long pieces of the primary orbit. This will enable us in Section 4 to prove a kind of numerical shadowing result: one finds true orbits in the neighborhood of the concatenated orbits which either solve an infinite or a finite boundary value problem. Detailed estimates in terms of the metric (12) are given. As in the introduction our assumptions are the following:

(A1) $f \in C^1(\mathbb{R}^d, \mathbb{R}^d)$.

(A2) There exist $\xi \in \mathbb{R}^d$ and $\bar{x}_\mathbb{Z} \in (\mathbb{R}^d)^\mathbb{Z}$ such that $\bar{x}_{n+1} = f(\bar{x}_n)$ for all $n \in \mathbb{Z}$, $\bar{x}_k \neq \xi$ for at least one $k \in \mathbb{Z}$ and $\lim_{n \to \pm\infty} \bar{x}_n = \xi$.

(A3) The point ξ is a hyperbolic fixed point of f, i.e. $Df(\xi)$ has no eigenvalues on the unit circle (but may have the eigenvalue zero).

(A4) The variational equation

$$u_{n+1} = Df(\bar{x}_n)u_n, \quad n \in \mathbb{Z} \tag{16}$$

has an exponential dichotomy on $\mathbb{Z}$ with data $(\bar{K}, \bar{\alpha}_{s,u}, \bar{P}_n^{s,u})$.

9

Condition **(A4)** guarantees hyperbolicity of the set $\mathcal{H}$, introduced in (2) and [42, Def. 1.1]. It is not difficult to show that Assumptions **(A1)**, **(A2)** and **(A4)** imply **(A3)**. However, **(A4)** does not follow from **(A1)**, **(A2)**, **(A3)** since it specifies a global property of the set $\mathcal{H}$. Let $Q^{s,u}$ be the projector onto the stable resp. unstable subspace of $Df(\xi)$. Then the autonomous variational equation

$$u_{n+1} = Df(\xi)u_n, \quad n \in \mathbb{Z} \tag{17}$$

has an exponential dichotomy on $\mathbb{Z}$ with associated projectors $Q^{s,u}$. Without loss of generality we may assume the same parameters $(\bar{K}, \bar{\alpha}_{s,u})$ as in **(A4)**. Moreover, the Roughness Theorem 20 applied to (16) and (17) on intervals $(-\infty, n_-] \cap \mathbb{Z}$ and $[n_+, \infty) \cap \mathbb{Z}$ with $-n_-, n_+$ sufficiently large, shows that the projectors satisfy

$$\bar{P}_n^{s,u} \to Q^{s,u} \quad \text{as} \quad n \to \pm\infty.$$

This fact will be essential for deriving Theorem 4 below.

3.1 The principal part of the homoclinic orbit and a particular pseudo-orbit

For proving our main results, it is important to fix the 'principle part' of the homoclinic orbit. For each $N \in \mathbb{N}$ we choose a position $a(N) \in \mathbb{Z}$ such that the interval $[a(N) + 1, a(N) + N - 1]$ contains the principle part of the homoclinic orbit $\bar{x}_{\mathbb{Z}}$ from **(A2)**. More formally, we define

$$b(N) := \min \left\{ b \in \mathbb{Z} : \sup_{n \notin [b+1, b+N-1]} \|\bar{x}_n - \xi\| \leq \sup_{n \notin [c+1, c+N-1]} \|\bar{x}_n - \xi\| \ \forall c \in \mathbb{Z} \right\}$$

and

$$a(N) := \begin{cases} b(N), & \text{if } \bar{x}_n \neq \xi \text{ for all } n \in \mathbb{Z}, \\ b(\lfloor \frac{N}{2} \rfloor), & \text{if } \bar{x}_n = \xi \text{ for some } n \in \mathbb{Z}. \end{cases}$$

The latter case occurs if the fixed point ξ has several pre-images and one of these pre-images coincides with an orbit point. If the fixed point has no stable eigenvalue, then this orbit is called a snap-back repeller in the literature, see [26]. An example of this kind is discussed in Section 6.4. The extra condition in the snap-back case guarantees convergence of the dichotomy projectors at the left and right boundary, see (28).

Figure 2 illustrates this choice of intervals in both cases.

From condition **(A2)** we deduce the first assertion of the following lemma.

Lemma 2 *Assume **(A1)**–**(A4)**.*

(i) *For each $\varepsilon > 0$ there exists an $N \in \mathbb{N}$ such that $\|\bar{x}_{a(N)+n} - \xi\| \leq \varepsilon$ for all $n \leq 0$ and for all $n \geq N$.*

(ii) *For any $N_1 \in \mathbb{N}$ there exists an $N_2 > N_1$ such that*

$$[a(N_1) + 1, a(N_1) + N_1 - 1] \subset [a(N_2) + 1, a(N_2) + N_2 - 1]. \tag{18}$$
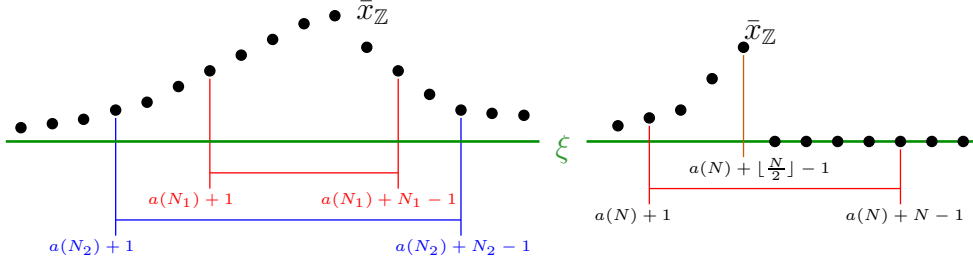
Figure 2: Choice of $a(N)$.

Proof: (of (ii)) First note that $\varepsilon_- = \sup_{n \notin [a(N_1)-1, a(N_1)+N_1-1]} \|\bar{x}_n - \xi\| > 0$ since $\bar{x}_n$ is nonconstant. Moreover, let $\varepsilon_+ = \|\bar{x}_{a(N_1)+N_1-1} - \xi\|$. If $\varepsilon_+ = 0$, then we are in the snap-back case and set $\varepsilon = \frac{1}{2}\varepsilon_-$, otherwise, we define $\varepsilon = \frac{1}{2}\min\{\varepsilon_-, \varepsilon_+\}$. Applying assertion (i) to this ε yields a number $N = N_2 > N_1$ with property (18). ∎

Let $J = [n_-, n_+]$, where the cases $n_- = -\infty$ and $n_+ = \infty$ are allowed and fix an $N \in \mathbb{N}$. Given a sequence of symbols $s_J \in \Sigma_{A(N)}^J$, we define the corresponding pseudo-orbit $\xi_J(s_J, N)$ as follows

$$\xi_n(s_J, N) := \begin{cases} \xi, & \text{if } s_n = 0, \\ \bar{x}_{a(N)+s_n}, & \text{otherwise}, \end{cases} \quad n \in J. \tag{19}$$

In what follows we study variational equations obtained by linearizing at orbits from the ε-neighborhoods

$$\mathcal{B}_\varepsilon(\xi_{\mathbb{Z}}(s_{\mathbb{Z}}, N)) := \{x_{\mathbb{Z}} \in (\mathbb{R}^d)^{\mathbb{Z}} : \|x_{\mathbb{Z}} - \xi_{\mathbb{Z}}(s_{\mathbb{Z}}, N)\|_\infty \le \varepsilon\}.$$

3.2 Uniform dichotomies of multi-humped pseudo-orbits

In the following we will concatenate two orbits each of which have exponential dichotomies, but for which the projectors at the interface do not coincide. This situation will be repaired by modifying the system matrix at the interface according to the following lemma.

Lemma 3 *Consider $B \in \mathbb{R}^{d,d}$ and three projectors $P_{-1}, P_0, Q_0 \in \mathbb{R}^{d,d}$ such that*

$$BP_{-1} = P_0 B. \tag{20}$$

Then the perturbed matrix

$$B_0 = (I + \Delta)B, \quad \Delta = 2Q_0 P_0 - P_0 - Q_0$$

satisfies

$$B_0 P_{-1} = Q_0 B_0 \tag{21}$$

and the estimate

$$\|\Delta\| \le (\|Q_0\| + \|P_0\|)\|P_0 - Q_0\|. \tag{22}$$

11

If $\|\Delta\| < 1$ and $B : \mathcal{R}(I - P_{-1}) \to \mathcal{R}(I - P_0)$ is invertible, then so is
$B_0 : \mathcal{R}(I - P_{-1}) \to \mathcal{R}(I - Q_0)$ and

$$\|(B_{0|\mathcal{R}(I-P_{-1})})^{-1}\| \leq \frac{1}{1 - \|\Delta\|} \|(B_{|\mathcal{R}(I-P_{-1})})^{-1}\|. \tag{23}$$

Proof: A direct computation shows

$$I + \Delta = Q_0 P_0 + (I - Q_0)(I - P_0) = I + Q_0(P_0 - Q_0) + (Q_0 - P_0)P_0. \tag{24}$$

From the first equality and (20) we obtain

$$B_0 P_{-1} = (I + \Delta)P_0 B = Q_0 P_0 B = Q_0(I + \Delta)B = Q_0 B_0,$$

while the second equality leads to the estimate (22). If $\|\Delta\| < 1$ it is clear that $I + \Delta$ is invertible with $\|(I + \Delta)^{-1}\| \leq \frac{1}{1-\|\Delta\|}$. Moreover, equation (24) shows that $I + \Delta$ maps $\mathcal{R}(I - P_0)$ into $\mathcal{R}(I - Q_0)$ and $\mathcal{R}(P_0)$ into $\mathcal{R}(Q_0)$ so that both projectors must have the same rank and $I + \Delta$ is a bijection between their ranges. We conclude that $B_0 = (I + \Delta)B : \mathcal{R}(I - P_{-1}) \to \mathcal{R}(I - Q_0)$ is invertible and satisfies the estimate (23). ∎

Our main result on persistence of exponential dichotomies is the following theorem.

Theorem 4 *Let conditions **(A1)**–**(A4)** be satisfied and let $0 < \alpha_{s,u} < \bar{\alpha}_{s,u}$.*

(i) *There exists an $N_{\mathrm{ED}} \in \mathbb{N}$ such that for all $N \geq N_{\mathrm{ED}}$ and for all $s_{\mathbb{Z}} \in \Sigma_{A(N)}^{\mathbb{Z}}$ the variational equation*

$$u_{n+1} = Df(\xi_n(s_{\mathbb{Z}}, N))u_n, \quad n \in \mathbb{Z} \tag{25}$$

has an exponential dichotomy with constants $(16\bar{K}^3, \alpha_{s,u})$.

(ii) *Fix $\bar{\varepsilon} > 0$. Then there exists an $\bar{N} \geq N_{\mathrm{ED}}$ such that for all $N \geq \bar{N}$, the dichotomy projectors $P_n^{s,u}$, $n \in \mathbb{Z}$ of (25) satisfy the inequalities for $n \in \mathbb{Z}$*

$$\begin{aligned}
\|P_n^{s,u} - Q^{s,u}\| &\leq \bar{\varepsilon}, & \text{if } s_n = 0, \\
\|P_n^{s,u} - \bar{P}_{a(N)+k}^{s,u}\| &\leq \bar{\varepsilon}, & \text{if } s_n = k \in \{1, \dots, N-1\}.
\end{aligned}$$

(iii) *Let $0 < \beta_{s,u} < \alpha_{s,u}$. Then, there exists an $\varepsilon_{\mathrm{ED}} > 0$ such that for all $N \geq N_{\mathrm{ED}}$, for all $s_{\mathbb{Z}} \in \Sigma_{A(N)}^{\mathbb{Z}}$ and for all $x_{\mathbb{Z}}, d_{\mathbb{Z}} \in (\mathbb{R}^d)^{\mathbb{Z}}$ with $x_{\mathbb{Z}}, x_{\mathbb{Z}} + d_{\mathbb{Z}} \in \mathcal{B}_{\varepsilon_{\mathrm{ED}}}(\xi_{\mathbb{Z}}(s_{\mathbb{Z}}, N))$, it follows that the difference equation*

$$u_{n+1} = \int_0^1 Df(x_n + \tau d_n)d\tau \cdot u_n, \quad n \in \mathbb{Z} \tag{26}$$

has an exponential dichotomy with constants $(32\bar{K}^3, \beta_{s,u})$ independent of $x_{\mathbb{Z}}$, $d_{\mathbb{Z}}$ and $s_{\mathbb{Z}}$.

Remark 5 *In case $d_n = 0$ for all $n \in \mathbb{Z}$, Theorem 4 (iii) proves a uniform exponential dichotomy of the variational equation*

$$u_{n+1} = Df(x_n)u_n, \quad n \in \mathbb{Z}$$

for all pseudo-orbits $x_{\mathbb{Z}} \in \mathcal{B}_{\varepsilon_{\mathrm{ED}}}(\xi_{\mathbb{Z}}(s_{\mathbb{Z}}, N))$.

A related result for invertible maps is proved by Palmer in [33, Theorem 2.1]. An exponential dichotomy on $\mathbb{Z}$ holds, if the difference equation has uniform dichotomies on all finite intervals $[b, b + M]$ with b from a suitable, relatively dense set of $\mathbb{Z}$.

Proof: The proof of (i) is based on the following idea: We begin with exponential dichotomies on the subintervals marked in red and black in Figure 3. Then, we invoke the repair mechanism from Lemma 3 with matrices $\Delta_{\pm}$ in order to combine these dichotomies to a dichotomy on $\mathbb{Z}$. Finally, an application of the Roughness Theorem 20 proves the desired dichotomy of the original equation.
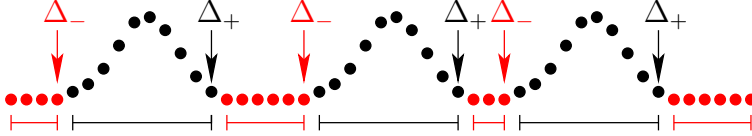

Figure 3: Illustration of the repair mechanism.

Step 1: Choice of constants. Fix $0 < \alpha_{s,u} < \hat{\alpha}_{s,u} < \bar{\alpha}_{s,u}$ and choose $N_0 \in \mathbb{N}$ such that

$$4\bar{K}^2 \mathrm{e}^{-(\bar{\alpha}_{s,u} - \hat{\alpha}_{s,u})N_0} < 1. \tag{27}$$

Define for $N \in \mathbb{N}$ the matrices

$$\Delta_-(N) := 2\bar{P}^s_{a(N)+1}Q^s - Q^s - \bar{P}^s_{a(N)+1}, \quad \Delta_+(N) := 2Q^s\bar{P}^s_{a(N)+N} - \bar{P}^s_{a(N)+N} - Q^s,$$

where $Q^{s,u}$ are the dichotomy projectors of (17). Then, it follows from Lemma 3, equation (22) that

$$\|\Delta_-(N)\| \leq 2\bar{K}\|\bar{P}^s_{a(N)+1} - Q^s\|, \quad \|\Delta_+(N)\| \leq 2\bar{K}\|\bar{P}^s_{a(N)+N} - Q^s\|$$

and these quantities converge to 0 as $N \to \infty$. Choose N_1 with

$$\max\{\|\Delta_-(N)\|, \|\Delta_+(N)\|\} \leq \tfrac{1}{2} \text{ for all } N \geq N_1 \tag{28}$$

and N_2 such that

$$\max\{\|\Delta_-(N)Df(\xi)\|, \|\Delta_+(N)Df(\bar{x}_{a(N)+N-1})\|\} \leq \gamma(8\bar{K}^3, \hat{\alpha}_{s,u}, \alpha_{s,u}) \tag{29}$$

holds for all $N \geq N_2$. Here, γ is the function from the Roughness Theorem 20. Finally, we define $N_{\mathrm{ED}} := \max\{N_0, N_1, N_2\}$.

Step 2: Definition of the repaired system. Let $N \geq N_{\mathrm{ED}}$ and $s_{\mathbb{Z}} \in \Sigma_{A(N)}^{\mathbb{Z}}$. We define for $n \in \mathbb{Z}$ the matrices $A_n := Df(\xi_n(s_{\mathbb{Z}}, N))$ and

$$B_n := \begin{cases} (I + \Delta_-(N))Df(\xi), & \text{if } s_{n+1} = 1, \\ (I + \Delta_+(N))Df(\bar{x}_{a(N)+N-1}), & \text{if } s_n = N - 1, \\ Df(\xi_n(s_{\mathbb{Z}}, N)), & \text{otherwise.} \end{cases}$$

Using (29), we conclude

$$\begin{aligned} \|A_n - B_n\| &= \begin{cases} \|\Delta_-(N)Df(\xi)\|, & \text{if } s_{n+1} = 1, \\ \|\Delta_+(N)Df(\bar{x}_{a(N)+N-1})\|, & \text{if } s_n = N - 1, \\ 0, & \text{otherwise} \end{cases} \\ &\leq \gamma(8\bar{K}^3, \hat{\alpha}_{s,u}, \alpha_{s,u}). \end{aligned}$$

The Roughness Theorem 20 yields the result (i), i.e. an exponential dichotomy with constants $(16\bar{K}^3, \alpha_{s,u})$ of the original system (25), if the repaired system

$$u_{n+1} = B_n u_n, \quad n \in \mathbb{Z} \tag{30}$$

has an exponential dichotomy with constants $(8\bar{K}^3, \hat{\alpha}_{s,u})$.

Step 3: System (30) has an exponential dichotomy on $\mathbb{Z}$ with constants $(8\bar{K}^3, \hat{\alpha}_{s,u})$. We introduce for $n \in \mathbb{Z}$ the projectors

$$\hat{P}_n^{s,u} := \begin{cases} Q^{s,u}, & \text{if } s_n = 0, \\ \bar{P}_{a(N)+k}^{s,u}, & \text{if } s_n = k \in \{1, \ldots, N - 1\}. \end{cases} \tag{31}$$

One immediately sees from equation (21) in Lemma 3 that these projectors satisfy the invariance condition (i) in Definition 18 w.r.t. the difference equation (30).

By the assumptions, the system (30) has exponential dichotomies on every subinterval (red or black in Figure 3) with constants $(\bar{K}, \bar{\alpha}_{s,u})$. Our construction shows that every subinterval can be enlarged by its right neighbor, where the dichotomy constant grows at most by $\|I + \Delta_\pm(N)\| \leq 2$ due to (28). Therefore, we have exponential dichotomies on the extended subintervals with projectors from (31) and constants $(2\bar{K}, \bar{\alpha}_{s,u})$.

Next we introduce the index set

$$\mathbb{Z}_1 = \{k \in \mathbb{Z} : s_k = 1\},$$

and for each $k \in \mathbb{Z}_1$ its successor and its predecessor by

$$\nu(k) = \inf\{\ell \in \mathbb{Z}_1 : \ell > k\}, \quad p(k) = \sup\{\ell \in \mathbb{Z}_1 : \ell < k\},$$

where $\nu(k) = \infty$ resp. $p(k) = -\infty$ if the corresponding sets are empty.

Denote by Φ the solution operator of (30). We prove the dichotomy estimate in forward time. For arbitrary $n \geq m$ let

$$k_- := \min\{[m, n] \cap \mathbb{Z}_1\}, \quad k_+ := \begin{cases} n, & \text{if } s_n = 0, \\ \max\{[m, n] \cap \mathbb{Z}_1\}, & \text{otherwise.} \end{cases}$$

14

It follows from (27) that

$$
\begin{aligned}
\|\Phi(n,m)\hat{P}_m^s\| &= \|\Phi(n,k_+)\hat{P}_{k_+}^s\Phi(k_+,k_-)\hat{P}_{k_-}^s\Phi(k_-,m)\hat{P}_m^s\| \\
&\leq \|\Phi(n,k_+)\hat{P}_{k_+}^s\|\|\Phi(k_-,m)\hat{P}_m^s\| \prod_{k\in\mathbb{Z}_1\cap[k_-,p(k_+)]} \|\Phi(\nu(k),k)\hat{P}_k^s\| \\
&\leq 2\bar{K}e^{-\bar{\alpha}_s(n-k_+)}\cdot 4\bar{K}^2e^{-\bar{\alpha}_s(k_--m)} \prod_{k\in\mathbb{Z}_1\cap[k_-,p(k_+)]} 4\bar{K}^2e^{-\bar{\alpha}_s(\nu(k)-k)} \\
&\leq 8\bar{K}^3e^{-\bar{\alpha}_s(n-k_++k_--m)} \\
&\quad \cdot \prod_{k\in\mathbb{Z}_1\cap[k_-,p(k_+)]} \left[4\bar{K}^2e^{-(\bar{\alpha}_s-\hat{\alpha}_s)(\nu(k)-k)}\right]\cdot e^{-\hat{\alpha}_s(\nu(k)-k)} \\
&\leq 8\bar{K}^3e^{-\bar{\alpha}_s(n-k_++k_--m)} \prod_{k\in\mathbb{Z}_1\cap[k_-,p(k_+)]} e^{-\hat{\alpha}_s(\nu(k)-k)} \\
&\leq 8\bar{K}^3e^{-\hat{\alpha}_s(n-m)}.
\end{aligned}
$$

In a similar fashion one gets for $n\geq m$

$$
\|\bar{\Phi}(m,n)\hat{P}_n^u\| \leq 8\bar{K}^3e^{-\hat{\alpha}_u(n-m)}.
$$

Thus, (30) has an exponential dichotomy on $\mathbb{Z}$ with data $(8\bar{K}^3,\hat{\alpha}_{s,u},\hat{P}_n^{s,u})$ and the proof of (i) is complete.

For proving (ii), choose an arbitrary $\bar{\varepsilon}>0$ and let $\mu=\mu(8\bar{K}^3,\hat{\alpha}_{s,u},\alpha_{s,u})$ be the function from the Roughness Theorem 20. Then, one finds an $\bar{N}\geq N_{\mathrm{ED}}$, such that

$$
\max\{\|\Delta_-(N)Df(\xi)\|,\|\Delta_+(N)Df(\bar{x}_{a(N)+N-1})\|\} \leq \frac{\bar{\varepsilon}}{16\bar{K}^3\mu} \quad \text{for all } N\geq\bar{N}.
$$

The Roughness Theorem 20 proves an exponential dichotomy for (25) with data $(16\bar{K}^3, \alpha_{s,u}, P_n^{s,u})$. The estimate (60) reads

$$
\begin{aligned}
\|P_n^{s,u}-\hat{P}_n^{s,u}\| &\leq 16\bar{K}^3\mu\max\{\|\Delta_-(N)Df(\xi)\|,\|\Delta_+(N)Df(\bar{x}_{a(N)+N-1})\|\} \\
&\leq 16\bar{K}^3\mu\frac{\bar{\varepsilon}}{16\bar{K}^3\mu} = \bar{\varepsilon}.
\end{aligned}
$$

Using the definition (31), our estimates follow.

For proving (iii), we recall the compact hyperbolic set $\mathcal{H}$ from (2) and choose Ω compact and sufficiently large such that $\mathrm{dist}(x,\mathcal{H})\leq 1$ implies $x\in\Omega$. Further, introduce the modulus of continuity

$$
\omega(Df,\Omega,\delta)=\sup\{\|Df(x)-Df(y)\|:x,y\in\Omega,\|x-y\|\leq\delta\}. \tag{32}
$$

Fix $N\geq N_{\mathrm{ED}}$ and $0<\beta_{s,u}<\alpha_{s,u}$. Choose $\varepsilon_{\mathrm{ED}}$ such that

$$
\Big\|\int_0^1 Df(x_n+\tau d_n)\mathrm{d}\tau - Df(\xi_n(s_\mathbb{Z},N))\Big\| \leq \omega(Df,\Omega,\varepsilon_{\mathrm{ED}}) \leq \gamma(16\bar{K}^3,\alpha_{s,u},\beta_{s,u})
$$

for all $s_{\mathbb{Z}} \in \Sigma^{\mathbb{Z}}_{A(N)}$ and for all $x_{\mathbb{Z}}, x_{\mathbb{Z}} + d_{\mathbb{Z}} \in \mathcal{B}_{\varepsilon_{\mathrm{ED}}}(\xi_{\mathbb{Z}}(s_{\mathbb{Z}}, N))$. Then, the Roughness Theorem 20 applies and proves an exponential dichotomy of (26) with constants $(32\bar{K}^3, \beta_{s,u})$. ∎

In the next section we need a result analogous to Theorem 4 for finite, but sufficiently large intervals $J \subset \mathbb{Z}$. The proof uses the same techniques and shows that the resulting data N_{ED}, $\varepsilon_{\mathrm{ED}}$ and $\bar{N} = \bar{N}(\bar{\varepsilon})$ as well as the dichotomy constants can be taken independently of J. For completeness, we state the theorem.

Theorem 6 *Let conditions **(A1)**–**(A4)** be satisfied and let $0 < \alpha_{s,u} < \bar{\alpha}_{s,u}$. Then, there exists an $\ell_0 > 0$ such that the assertions (i)-(iii) of Theorem 4 hold for all intervals $J = [n_-, n_+]$ with $n_+ - n_- \geq \ell_0$.*

4 Multi-humped orbits on finite and infinite intervals

In this section, we prove existence of a multi-humped homoclinic orbit w.r.t. each finite or infinite coding sequence. In all considerations of the following sections, we fix parameters $0 < \alpha_{s,u} < \bar{\alpha}_{s,u}$ and $0 < \beta_{s,u} < \alpha_{s,u}$.

4.1 Solutions of boundary value problems

Let $J = [n_-, n_+]$, $\tilde{J} = [n_-, n_+ - 1]$ be either a finite interval or let $J = \tilde{J} = \mathbb{Z}$. We define the operator

$$\Gamma_J(x_J) = \begin{pmatrix} x_{n+1} - f(x_n), & n \in \tilde{J}, \\ b(x_{n_-}, x_{n_+}), & \text{if } J \text{ is finite} \end{pmatrix}.$$

We impose the following condition on the boundary operator.

(A5) The operator b satisfies $b \in \mathcal{C}^1(\mathbb{R}^{2d}, \mathbb{R}^d)$ and $b(\xi, \xi) = 0$. Furthermore, the linear map

$$B := \begin{pmatrix} D_1 b(\xi, \xi)_{|\mathcal{R}(Q^s)} & D_2 b(\xi, \xi)_{|\mathcal{R}(Q^u)} \end{pmatrix} : \mathcal{R}(Q^s) \oplus \mathcal{R}(Q^u) \to \mathbb{R}^d$$

is invertible, where $Q^{s,u}$ are the dichotomy projectors from (17).

Examples of boundary operators, satisfying **(A5)** are

- periodic boundary conditions $b_{\mathrm{per}}(x, y) := x - y$,

- projection boundary conditions $b_{\mathrm{proj}}(x, y) := \begin{pmatrix} Y_s^T(x - \xi) \\ Y_u^T(y - \xi) \end{pmatrix}$, where $Y_{s,u}$ are bases of $(\mathcal{R}(Q^{u,s}))^\perp$, respectively.

Now, we have all tools at hand to prove our main existence theorem for finite and infinite homoclinic orbits.

Theorem 7 *Assume **(A1)**–**(A5)**. Then there exists a constant $\varepsilon_{\mathrm{sol}}$ and for any $0 < \varepsilon \leq \varepsilon_{\mathrm{sol}}$ a number N_ε, such that for all $N \geq N_\varepsilon$ the following property holds true for both $J = \mathbb{Z}$ and J finite with $|J| \geq N + 1$:*

For any $s_J \in \Sigma^J_{A(N)}$, the operator Γ_J has a unique zero $x_J \in \mathcal{B}_\varepsilon(\xi_J(s_J, N))$, where the pseudo-orbit $\xi_J(s_J, N)$ is defined in (19). Furthermore, $\mathcal{B}_\varepsilon(\xi_J(s_J^1, N)) \cap \mathcal{B}_\varepsilon(\xi_J(s_J^2, N)) = \emptyset$ for any $s_J^1 \neq s_J^2 \in \Sigma^J_{A(N)}$.

Proof: *Step 1: Choice of constants.* Theorems 4, 6 give constants $\varepsilon_{\mathrm{ED}}$ and N_{ED} such that the dichotomy rates of the variational equation w.r.t. the pseudo-orbit $\xi_J(s_J, N)$, $N \geq N_{\mathrm{ED}}$ do not depend on the specific sequence s_J. As a consequence, we get uniform estimates for the corresponding Green's function, defined in (58) with $K = 16\bar{K}^3$, $n \in J$:

$$
\begin{aligned}
\left\| \sum_{m \in J} G(n, m) \right\| &\leq \sum_{m=-\infty}^{n} K\mathrm{e}^{-\alpha_s(n-m)} + \sum_{m=n+1}^{\infty} K\mathrm{e}^{-\alpha_u(m-n)} \\
&= K\left(\frac{1}{1 - \mathrm{e}^{-\alpha_s}} + \frac{\mathrm{e}^{-\alpha_u}}{1 - \mathrm{e}^{-\alpha_u}} \right) =: C_G.
\end{aligned}
$$

In the following let $C_{B^{-1}} = C_b = 1$ if $J = \mathbb{Z}$, and define $C_{B^{-1}} := \max\{\|B^{-1}\|, 1\}$ with B from **(A5)**, $C_b := \max\{\|D_1 b(\xi, \xi)\|, \|D_2 b(\xi, \xi)\|, 1\}$ if J is finite.

Applying assertion (ii) of Theorem 6 with $\bar{\varepsilon} = \frac{1}{2}$, we find an $N_0 \geq N_{\mathrm{ED}}$, such that the system (25) has an exponential dichotomy on the interval $J = [n_-, n_+]$ for all $N \geq N_0$ and $s_J \in \Sigma_{A(N)}^J$. The corresponding projectors $P_n^{s,u}$ depend on s_J, but satisfy uniform estimates. Note that $s_J \in \Sigma_{A(N)}^J$ and hence, $s_{n_-} = s_{n_+} = 0$ and $\|Q^s - P_{n_-}^s\| \leq \frac{1}{2}$ and $\|Q^u - P_{n_+}^u\| \leq \frac{1}{2}$ due to Theorem 6 (ii).

We define

$$
\begin{aligned}
T_{n_-}^s &:= I + Q^s - P_{n_-}^s : \mathcal{R}(P_{n_-}^s) \to \mathcal{R}(Q^s), \\
T_{n_+}^u &:= I + Q^u - P_{n_+}^u : \mathcal{R}(P_{n_+}^u) \to \mathcal{R}(Q^u)
\end{aligned}
$$

and observe that these matrices are invertible with uniformly bounded inverse $\|(T_{n_-}^s)^{-1}\| \leq 2$, $\|(T_{n_+}^u)^{-1}\| \leq 2$. Let $B_J = \begin{pmatrix} A_{n_-} & A_{n_+} \end{pmatrix}$ with

$$
\begin{aligned}
A_{n_-} &= D_1 b(\xi, \xi)(T_{n_-}^s)^{-1}_{|\mathcal{R}(Q^s)} + D_2 b(\xi, \xi)\Phi(n_+, n_-)(T_{n_-}^s)^{-1}_{|\mathcal{R}(Q^s)}, \\
A_{n_+} &= D_2 b(\xi, \xi)(T_{n_+}^u)^{-1}_{|\mathcal{R}(Q^u)} + D_1 b(\xi, \xi)\bar{\Phi}(n_-, n_+)(T_{n_+}^u)^{-1}_{|\mathcal{R}(Q^u)}.
\end{aligned}
$$

The second terms decay exponentially as $n_\pm \to \pm\infty$, due to the uniform dichotomy rates, while the first terms converge to $D_1 b(\xi, \xi)_{|\mathcal{R}(Q^s)}$ and $D_2 b(\xi, \xi)_{|\mathcal{R}(Q^u)}$ respectively, as $n_\pm \to \pm\infty$. Thus, there exists $N_1 \geq N_0$, such that for all $N \geq N_1$ the estimate $\|B_J - B\| \leq \frac{1}{2C_{B^{-1}}}$ holds.

Let $\eta = (17KC_{B^{-1}}C_b C_G)^{-1}$. Using the modulus of continuity from (32), there exists an $\tilde{\varepsilon}$ such that

$$
\begin{aligned}
\omega(Df, \Omega, \tilde{\varepsilon}) &\leq \frac{\eta}{2}, \\
\|Db(y, z) - Db(\xi, \xi)\| &\leq \frac{\eta}{2} \quad \text{for all } y, z \in \mathcal{B}_{\tilde{\varepsilon}}(\xi).
\end{aligned}
\tag{33}
$$

Choose $\hat{\varepsilon} > 0$ such that

$$
\max_{n \in [a(N_{\mathrm{ED}})+1, a(N_{\mathrm{ED}})+N_{\mathrm{ED}}-1]} \min_{m \in \mathbb{Z}, m \neq n} \|\bar{x}_n - \bar{x}_m\| > 2\hat{\varepsilon}.
\tag{34}
$$

Fix $\varepsilon_{\mathrm{sol}} = \min\{\varepsilon_{\mathrm{ED}}, \tilde{\varepsilon}, \hat{\varepsilon}\}$ and let $\varepsilon \leq \varepsilon_{\mathrm{sol}}$.

Using Lemma 2 (i), we find an $N_\varepsilon \geq N_1$ such that we get for all $N \geq N_\varepsilon$

$$
\|\bar{x}_{a(N)+n} - \xi\| \leq \frac{\eta}{2}\varepsilon \quad \text{for all} \quad n \leq 1 \text{ and } n \geq N.
\tag{35}
$$

Fix $N \geq N_\varepsilon$, let J be an interval, $|J| \geq N + 1$ and choose an arbitrary sequence of symbols $s_J \in \Sigma^J_{A(N)}$. By Theorems 4, 6 the variational equation along the corresponding pseudo-orbit $\xi_J(s_J, N)$ has an exponential dichotomy with data $(K, \alpha_{s,u}, P^{s,u}_n)$.

Step 2: $D\Gamma_J(\xi_J(s_J, N))$ is invertible with inverse uniformly bounded by η^{-1}. For $y_{\tilde{J}} \in \mathcal{S}_{\tilde{J}}$ and $r \in \mathbb{R}^d$ solve the boundary value problem

$$D\Gamma_J(\xi_J(s_J, N))u_J = \begin{pmatrix} y_{\tilde{J}} \\ r \end{pmatrix} \Leftrightarrow \begin{cases} u_{n+1} - Df(\xi_n(s_J, N))u_n = y_n, \ n \in \tilde{J}, \\ D_1 b(\xi, \xi)u_{n_-} + D_2 b(\xi, \xi)u_{n_+} = r, \end{cases} \quad (36)$$

where the second row vanishes if $J = \mathbb{Z}$. Here, $\mathcal{S}_J$ denotes the Banach space of bounded sequences on J, cf. Appendix A.1. The general solution of the linear equation is given by

$$u_n = \Phi(n, n_-)v_- + \bar{\Phi}(n, n_+)v_+ + \sum_{m \in \tilde{J}} G(n, m+1)y_m, \ v_- \in \mathcal{R}(P^s_{n_-}), \ v_+ \in \mathcal{R}(P^u_{n_+}). \quad (37)$$

In case $J = \mathbb{Z}$, the first two terms are equal to 0 and the third term defines the unique bounded solution on $\mathbb{Z}$. In the finite case, we plug (37) into the boundary condition in (36) and guarantee in this way uniqueness of the solution. Then, we transform the system into $n_\pm$-independent spaces by introducing the variables $\bar{v}_- = T^s_{n_-}v_-$ and $\bar{v}_+ = T^u_{n_+}v_+$. In the new coordinates, the resulting system reads

$$B_J \begin{pmatrix} \bar{v}_- \\ \bar{v}_+ \end{pmatrix} = R,$$

where

$$R = r - D_1 b(\xi, \xi) \sum_{m \in \tilde{J}} G(n_-, m+1)y_m - D_2 b(\xi, \xi) \sum_{m \in \tilde{J}} G(n_+, m+1)y_m,$$

$$\|R\| \leq \|r\| + 2C_b C_G \|y_{\tilde{J}}\|_\infty.$$

Since $\|B_J - B\| \leq \frac{1}{2C_{B^{-1}}}$, the Banach Lemma applies and guarantees that B_J is invertible and $\|B_J^{-1}\| \leq 2C_{B^{-1}}$. Furthermore the following estimates hold true:

$$\|v_\pm\| \leq 2\|\bar{v}_\pm\| \leq 4C_{B^{-1}}\|r\| + 8C_{B^{-1}}C_b C_G \|y_{\tilde{J}}\|_\infty.$$

This implies that for all $n \in J$,

$$\begin{aligned} \|u_n\| &\leq 8KC_{B^{-1}}\|r\| + 16KC_{B^{-1}}C_b C_G \|y_{\tilde{J}}\|_\infty + C_G \|y_{\tilde{J}}\|_\infty \\ &\leq 17KC_{B^{-1}}C_b C_G(\|r\| + \|y_{\tilde{J}}\|_\infty) = \eta^{-1}(\|y_{\tilde{J}}\|_\infty + \|r\|) \end{aligned}$$

and consequently

$$\|D\Gamma_J(\xi_J(s_J, N))^{-1}\| \leq \eta^{-1}.$$

Step 3: Existence of a unique solution in $\mathcal{B}_\varepsilon(\xi_J(s_J, N))$. We apply the Lipschitz Inverse Mapping Theorem 21 with the setting

$$Y = (\mathcal{S}_J, \|\cdot\|_\infty), \ Z = (\mathcal{S}_{\tilde{J}} \times \mathbb{R}^d, \max\{\|\cdot\|_\infty, \|\cdot\|\}), \ F = \Gamma_J, \ y_0 = \xi_J(s_J, N)$$

and in case $J = \mathbb{Z}$ we define $Z = (\mathcal{S}_{\mathbb{Z}}, \|\cdot\|_\infty)$. Finally, we choose $\delta = \varepsilon$ and $\kappa = \frac{\eta}{2}$.

Assumption (63) is satisfied, since by (33) we find that

$$
\|D\Gamma_J(z_J) - D\Gamma_J(\xi_J(s_J, N))\| \leq \max\{\sup_{n\in\tilde{J}} \|Df(z_n) - Df(\xi_n(s_J, N))\|,
$$
$$
\|Db(z_{n_-}, z_{n_+}) - Db(\xi, \xi)\|\} \leq \tfrac{\eta}{2}
$$

holds for all $z_J \in \mathcal{B}_\varepsilon(\xi_J(s_J, N))$.

Assumption (64) follows from (35):

$$
\|\Gamma_J(\xi_J(s_J, N))\| = \|(\xi_{n+1}(s_J, N) - f(\xi_n(s_J, N)))_{n\in\tilde{J}}\|_\infty
$$
$$
= \max\left\{\|\bar{x}_{a(N)+1} - \xi\|, \|\xi - \bar{x}_{a(N)+N}\|\right\} \leq \tfrac{\eta}{2}\varepsilon.
$$

Thus, Theorem 21 proves that Γ_J has a unique zero $x_J \in \mathcal{B}_\varepsilon(\xi_J(s_J, N))$.

Step 4: $\mathcal{B}_\varepsilon(\xi_J(s_J^1, N)) \cap \mathcal{B}_\varepsilon(\xi_J(s_J^2, N)) = \emptyset$ *for any* $s_J^1 \neq s_J^2 \in \Sigma_{A(N)}^J$. From (34), we conclude the existence of an $\ell \in [1, N_{\mathrm{ED}} - 1]$ such that

$$
\mathcal{B}_\varepsilon(\xi_n(s_J^1, N)) \cap \mathcal{B}_\varepsilon(\xi_n(s_J^2, N)) = \emptyset \quad \text{for all } n \text{ satisfying } s_n^1 = \ell, \ s_n^2 \neq \ell. \tag{38}
$$

Let $s_J^1 \neq s_J^2 \in \Sigma_{A(N)}^J$. Then, there exists an $m \in J$ such that $0 = s_m^1 \neq s_m^2 = k \in [1, N-1]$. It follows that $s_{m+\ell-k}^2 = \sigma^{\ell-k}(s_m^2) = \sigma^{\ell-k}(k) = k + \ell - k = \ell$. On the other hand, $s_{m+\ell-k}^1 \neq \ell$ since $s_{m+\ell-k}^1 = \ell$ implies $s_m^1 = \sigma^{k-\ell}(s_{m+\ell-k}^1) = \sigma^{k-\ell}(\ell) = k$, a contradiction. Using (38), the claim follows. ∎

4.2 Exponential decay of errors

Precise error estimates are based on the fact that all orbits in $\mathcal{B}_\varepsilon(\xi_J(s_J, N))$ converge in the interior of J exponentially fast towards each other with a uniform rate.

Theorem 8 *Assume **(A1)**–**(A4)**, then the following statement holds for all* $0 < \varepsilon \leq \varepsilon_{\mathrm{ED}}$, $N \geq N_{\mathrm{ED}}$, $|J| \geq N+1$.

Any two finite orbit segments $z_J^1, z_J^2 \in \mathcal{B}_\varepsilon(\xi_J(s_J, N))$ *satisfy the estimate*

$$
\|z_n^1 - z_n^2\| \leq L\varepsilon \left(e^{-\beta_s(n-n_-)} + e^{-\beta_u(n_+-n)}\right), \quad n \in J, \quad L := 64\bar{K}^3 \tag{39}
$$

with constants $\varepsilon_{\mathrm{ED}}, N_{\mathrm{ED}}$ *and* $\beta_{s,u}$ *from Theorem 6 (iii).*

Proof: For $z_J^1, z_J^2 \in \mathcal{B}_\varepsilon(\xi_J(s_J, N))$, define $d_J = z_J^1 - z_J^2$. Then, d_J solves the difference equation

$$
d_{n+1} = z_{n+1}^1 - z_{n+1}^2 = f(z_n^1) - f(z_n^2) = \int_0^1 Df(z_n^2 + \tau d_n)\mathrm{d}\tau \cdot d_n
$$
$$
= A_n d_n, \quad n \in \tilde{J}.
$$

Note that $z_n^2 + \tau d_n \in \mathcal{B}_\varepsilon(\xi_n(s_J, N))$ for all $n \in J$ and all $\tau \in [0,1]$. Thus, Theorem 6 (iii) applies and yields an exponential dichotomy of the difference equation

$$
u_{n+1} = A_n u_n, \quad n \in \tilde{J} \tag{40}
$$

with uniform constants $\frac{L}{2} = 32\bar{K}^3$, $\beta_{s,u}$ and projectors $Q_n^{s,u}$. Denote by Φ the solution operator of (40). Since d_J is a solution of (40) we conclude

$$d_n = \Phi(n, n_-)Q_{n_-}^s d_{n_-} + \bar{\Phi}(n, n_+)Q_{n_+}^u d_{n_+}, \quad n \in J$$

and

$$
\begin{aligned}
\|d_n\| &\leq \tfrac{L}{2}\mathrm{e}^{-\beta_s(n-n_-)}\|d_{n_-}\| + \tfrac{L}{2}\mathrm{e}^{-\beta_u(n_+-n)}\|d_{n_+}\| \\
&\leq L\varepsilon \left(\mathrm{e}^{-\beta_s(n-n_-)} + \mathrm{e}^{-\beta_u(n_+-n)}\right).
\end{aligned}
$$

∎

For a given sequence $s_J \in \Sigma_{A(N)}^J$, the choice of a boundary condition in **(A5)** leads to a unique zero z_J^1 of Γ_J in $\mathcal{B}_\varepsilon(\xi_J(s_J, N))$, cf. Theorem 7. Changing the boundary condition results in an alternative orbit segment $z_J^2 \in \mathcal{B}_\varepsilon(\xi_J(s_J, N))$. The error estimate (39) shows that the influence of the boundary condition is only over a short range. For a similar observation in nonautonomous systems, we refer to [19, Theorem 5].

Combining Theorem 7 and Theorem 8 we immediately obtain the following approximation result for multi-humped homoclinic orbits.

Corollary 9 *Assume **(A1)**–**(A5)**. Let $0 < \varepsilon \leq \varepsilon_{\mathrm{sol}}$ and N_ε be given as in Theorem 7. Consider a finite interval $J = [n_-, n_+]$ with $|J| \geq N + 1$ and $N \geq N_\varepsilon$. For any sequence of symbols $s_\mathbb{Z} \in \Sigma_{A(N)}^\mathbb{Z}$ such that $s_{n_-} = s_{n_+} = 0$ denote by $\xi_\mathbb{Z}(s_\mathbb{Z}, N)$ the pseudo-orbit, defined in (19).*

Then there exist unique orbits $x_\mathbb{Z} \in \mathcal{B}_\varepsilon(\xi_\mathbb{Z}(s_\mathbb{Z}, N))$ and $y_J \in \mathcal{B}_\varepsilon(\xi_J(s_J, N))$, satisfying

$$\Gamma_\mathbb{Z}(x_\mathbb{Z}) = 0, \quad \Gamma_J(y_J) = 0,$$

respectively. Furthermore, approximation errors can be estimated as

$$\|x_n - y_n\| \leq L\varepsilon \left(\mathrm{e}^{-\beta_s(n-n_-)} + \mathrm{e}^{-\beta_u(n_+-n)}\right), \quad n \in J.$$

4.3 Hausdorff distance between finite and infinite orbits

Choose $0 < \varepsilon \leq \varepsilon_{\mathrm{sol}}$, $N \geq N_\varepsilon$ as in Theorem 7. We define the set of all infinite and finite multi-humped orbits for sufficiently large finite intervals J, $|J| \geq N + 1$:

$$
\begin{aligned}
\mathcal{X}_J(N, \varepsilon) &= \{x_J \in \Omega^J : \exists s_J \in \Sigma_{A(N)}^J : x_J \in \mathcal{B}_\varepsilon(\xi_J(s_J, N)), \Gamma_J(x_J) = 0\}, \\
\mathcal{X}(N, \varepsilon) &= \{x_\mathbb{Z} \in \Omega^\mathbb{Z} : \exists s_\mathbb{Z} \in \Sigma_{A(N)}^\mathbb{Z} : x_\mathbb{Z} \in \mathcal{B}_\varepsilon(\xi_\mathbb{Z}(s_\mathbb{Z}, N)), \Gamma_\mathbb{Z}(x_\mathbb{Z}) = 0\}. \quad (41)
\end{aligned}
$$

Theorem 10 *Assume **(A1)**–**(A5)**. Fix $0 < \varepsilon \leq \varepsilon_{\mathrm{sol}}$, $N \geq N_\varepsilon$ as in Theorem 7. For any $\delta > 0$ there exists an $\bar{n} > 0$ such that for all $J = [n_-, n_+]$ with $-n_-, n_+ \geq \bar{n}$ and $n_+ - n_- \geq 3N + 1$ the following assertion holds*

$$\mathrm{dist}_{\mathrm{H}}(\mathcal{X}(N, \varepsilon)_{|J} - \mathcal{X}_J(N, \varepsilon)) \leq \delta.$$

Here, $\mathcal{X}(N, \varepsilon)_{|J}$ is the set of sequences from $\mathcal{X}(N, \varepsilon)$, restricted to the finite interval J and $\mathrm{dist}_{\mathrm{H}}$ is the Hausdorff distance (11) with the dist-function defined in (12).

Proof: Let Ω be the compact neighborhood of the homoclinic orbit from Theorem 4 and let $C = \text{diam}(\Omega)$. Further, denote by $(\frac{L}{2} = 32\bar{K}^3, \beta_{s,u})$ the uniform dichotomy data, which Theorems 4, 6 (iii) provides for the variational equations along any orbit $x_{\mathbb{Z}} \in \mathcal{X}(N, \varepsilon)$. For fixed $\delta > 0$ we choose $\bar{n}$ such that

$$\max\left\{ C \sum_{n \in J \setminus \hat{J}} 2^{-|n|} + L\varepsilon \sum_{n \in \hat{J}} 2^{-|n|} \left(e^{-\beta_s(n - n_- - N)} + e^{-\beta_u(n_+ - N - n)} \right), \right.$$
$$\left. L\varepsilon \sum_{n \in J} 2^{-|n|} \left(e^{-\beta_s(n - n_-)} + e^{-\beta_u(n_+ - n)} \right) \right\} \leq \delta$$

for $J = [n_-, n_+]$, $\hat{J} = [n_- + N, n_+ - N]$, $-n_-, n_+ \geq \bar{n}$, $n_+ - n_- \geq 3N + 1$. Note the different directions of exponential decay in the second and third sum.

Step 1: For any $x_J \in \mathcal{X}(N, \varepsilon)_{|J}$ there exists a $y_J \in \mathcal{X}_J(N, \varepsilon)$ such that $\text{dist}(x_J, y_J) \leq \delta$, where the distance between two segments is defined in (12). For $x_{\mathbb{Z}} \in \mathcal{X}(N, \varepsilon)$ let $s_{\mathbb{Z}} \in \Sigma^{\mathbb{Z}}_{A(N)}$ be the corresponding sequence of symbols. Since its restriction to the finite interval J does not necessarily lie in $\mathcal{X}_J(N, \varepsilon)$, we introduce an adapted cutoff process. Let $i_- = \max\{n \in [n_-, n_- + N] : s_n = 0\}$, $i_+ = \min\{n \in [n_+ - N, n_+] : s_n = 0\}$ and define for $n \in J$

$$\hat{s}_n = \left\{ \begin{array}{ll} s_n, & \text{for } n \in [i_-, i_+], \\ 0, & \text{otherwise.} \end{array} \right.$$

For the sequence $\hat{s}_J$, the existence of an orbit $y_J \in \mathcal{X}_J(N, \varepsilon)$ follows from Theorem 7. Estimates for the difference of these orbits are due to Theorem 8:

$$\|x_n - y_n\| \leq L\varepsilon \left(e^{-\beta_s(n - n_- - N)} + e^{-\beta_u(n_+ - N - n)} \right), \quad n \in \hat{J},$$
$$\|x_n - y_n\| \leq C, \quad n \in J \setminus \hat{J}.$$

Combining these estimates we obtain

$$\text{dist}(x_J, y_J) = \sum_{n \in J} 2^{-|n|} \|x_n - y_n\|$$
$$\leq C \sum_{n \in J \setminus \hat{J}} 2^{-|n|} + L\varepsilon \sum_{n \in \hat{J}} 2^{-|n|} \left(e^{-\beta_s(n - n_- - N)} + e^{-\beta_u(n_+ - N - n)} \right) \leq \delta.$$

Step 2: For any $x_J \in \mathcal{X}_J(N, \varepsilon)$ there exists a $y_J \in \mathcal{X}(N, \varepsilon)_{|J}$ such that $\text{dist}(x_J, y_J) \leq \delta$. Let $x_J \in \mathcal{X}_J(N, \varepsilon)$ and let $s_J \in \Sigma^J_{A(N)}$ be the corresponding symbolic sequence. Define for $n \in \mathbb{Z}$

$$\tilde{s}_n = \left\{ \begin{array}{ll} s_n, & \text{for } n \in J, \\ 0, & \text{otherwise.} \end{array} \right.$$

Since $s_{n_-} = s_{n_+} = 0$ this setting leads to $\tilde{s} \in \Sigma^{\mathbb{Z}}_{A(N)}$. By Theorem 7 we obtain an orbit $y_{\mathbb{Z}} \in \mathcal{X}(N, \varepsilon)$ which belongs to the sequence $\tilde{s}_{\mathbb{Z}}$, and Theorem 8 gives the estimate

$$\|x_n - y_n\| \leq L\varepsilon \left(e^{-\beta_s(n - n_-)} + e^{-\beta_u(n_+ - n)} \right), \quad n \in J.$$

Thus, we get

$$\text{dist}(x_J, y_J) \leq L\varepsilon \sum_{n \in J} 2^{-|n|} \left(e^{-\beta_s(n - n_-)} + e^{-\beta_u(n_+ - n)} \right) \leq \delta.$$

∎

5 The Homoclinic Theorem for finite and infinite orbits in non-invertible systems

In this section we show how the Homoclinic Theorem for noninvertible maps ([42], [22]) can be derived in a straightforward manner from the results of Section 4. In addition we prove an analogous theorem for finite orbits segments of sufficient length. The idea is to first prove the conjugacy of a subshift with the map $\mathcal{F}$ (see (4)), induced by f on the solution set $\mathcal{X}(N, \varepsilon)$ from (41). Then one shows that the solution set coincides with the orbit set $\mathrm{Orb}(\mathcal{O})$ from (3) for a properly chosen neighborhood $\mathcal{O}$. This approach will then be transferred to finite orbit segments J for a suitably defined operator $\mathcal{F}_J$, see (10).

5.1 Conjugacy between shift-dynamics and the dynamics on $\mathcal{X}(N, \varepsilon)$

Instead of directly considering the maximal invariant set $\mathrm{Orb}(\mathcal{O})$, it is advantageous to start with the set $\mathcal{X}(N, \varepsilon)$, defined in (41) with $\varepsilon \leq \varepsilon_{\mathrm{sol}}$ and $N \geq N_\varepsilon$. Exploiting the results from the previous section, we prove the existence of a homeomorphism h, which conjugates the subshift σ on $\Sigma^{\mathbb{Z}}_{A(N)}$ to the orbit shift $\mathcal{F}$ on $\mathcal{X}(N, \varepsilon)$, cf. (4):

$$\begin{array}{ccc} \Sigma^{\mathbb{Z}}_{A(N)} & \xrightarrow{\sigma} & \Sigma^{\mathbb{Z}}_{A(N)} \\ {\scriptstyle h}\downarrow & & \downarrow{\scriptstyle h} \\ \mathcal{X}(N, \varepsilon) & \xrightarrow{\mathcal{F}} & \mathcal{X}(N, \varepsilon) \end{array} \qquad (42)$$

Theorem 11 *Assume **(A1)**–**(A4)**. Let $0 < \varepsilon \leq \varepsilon_{\mathrm{sol}}$, $N \geq N_\varepsilon$ as in Theorem 7. Then there exists a homeomorphism h, such that the diagram (42) commutes, i.e. $\mathcal{F} \circ h = h \circ \sigma$.*

Proof: Fix $0 < \varepsilon \leq \varepsilon_{\mathrm{sol}}$ and $N \geq N_\varepsilon$.

   Step 1: Definition of $h : \Sigma^{\mathbb{Z}}_{A(N)} \to \mathcal{X}(N, \varepsilon)$. It follows from Theorem 7 that for any $s_{\mathbb{Z}} \in \Sigma^{\mathbb{Z}}_{A(N)}$, there exists a unique $x_{\mathbb{Z}}(s_{\mathbb{Z}}) \in \mathcal{B}_\varepsilon(\xi_{\mathbb{Z}}(s_{\mathbb{Z}}, N))$ such that $\Gamma_{\mathbb{Z}}(x_{\mathbb{Z}}(s_{\mathbb{Z}})) = 0$. We define

$$h(s_{\mathbb{Z}}) := x_{\mathbb{Z}}(s_{\mathbb{Z}}), \quad s_{\mathbb{Z}} \in \Sigma^{\mathbb{Z}}_{A(N)}.$$

   Step 2: h is invertible. By definition, for each $x_{\mathbb{Z}} \in \mathcal{X}(N, \varepsilon)$ there exists an $s_{\mathbb{Z}} \in \Sigma^{\mathbb{Z}}_{A(N)}$ such that $h(s_{\mathbb{Z}}) = x_{\mathbb{Z}}$. Furthermore, Theorem 7 guarantees uniqueness of $s_{\mathbb{Z}}$, since $B_\varepsilon(\xi_{\mathbb{Z}}(s_{\mathbb{Z}}, N)) \cap B_\varepsilon(\xi_{\mathbb{Z}}(\tilde{s}_{\mathbb{Z}}, N)) = \emptyset$ for any $s_{\mathbb{Z}} \neq \tilde{s}_{\mathbb{Z}} \in \Sigma^{\mathbb{Z}}_{A(N)}$.

   Step 3: h and h^{-1} are continuous. Let $C = \mathrm{diam}(\Omega)$ and $\frac{L}{2} = 32\bar{K}^3$, $\beta_{s,u}$ be the uniform dichotomy constant for the variational equation along each $x_{\mathbb{Z}} \in \mathcal{X}(N, \varepsilon)$, cf. Theorem 4 (iii).

   For any fixed $\delta_1 > 0$, careful estimates show there exist integers $n_- < 0 < n_+$ such that the following estimates hold for $J = [n_-, n_+]$,

$$C \sum_{n \in \mathbb{Z} \setminus J} 2^{-|n|} + L\varepsilon \sum_{n \in J} 2^{-|n|} \left(e^{-\beta_s(n - n_-)} + e^{-\beta_u(n_+ - n)} \right) \leq \delta_1.$$

Choose $\delta_2 < 2^{-\max\{-n_-, n_+\}}$. For all $s_{\mathbb{Z}}^{1,2} \in \Sigma_{A(N)}^{\mathbb{Z}}$ satisfying

$$d(s_{\mathbb{Z}}^1, s_{\mathbb{Z}}^2) = \sum_{n \in \mathbb{Z}} 2^{-|n|} |s_n^1 - s_n^2| \le \delta_2$$

we conclude $s_n^1 = s_n^2$ for all $n \in J$. Applying Theorem 8 on the interval J with the boundary operator b_{proj} gives the estimate

$$\|h(s_{\mathbb{Z}}^1)_n - h(s_{\mathbb{Z}}^2)_n\| \le L\varepsilon \left(e^{-\beta_s(n - n_-)} + e^{-\beta_u(n_+ - n)} \right) \quad \text{for } n \in J.$$

Inserting this into the dist-function and applying a global estimate outside the finite interval J, we obtain

$$\text{dist}(h(s_{\mathbb{Z}}^1), h(s_{\mathbb{Z}}^2)) \le C \sum_{n \in \mathbb{Z} \setminus J} 2^{-|n|} + L\varepsilon \sum_{n \in J} 2^{-|n|} \left(e^{-\beta_s(n - n_-)} + e^{-\beta_u(n_+ - n)} \right) \le \delta_1.$$

This proves continuity of h, and then continuity of h^{-1} follows from the compactness of $\Sigma_{A(N)}^{\mathbb{Z}}$ and the Hausdorff property of $\mathcal{X}(N, \varepsilon)$.

    Step 4: Proof of conjugacy. Let $s_{\mathbb{Z}} \in \Sigma_{A(N)}^{\mathbb{Z}}$. Then, $x_{\mathbb{Z}} = h(s_{\mathbb{Z}}) \in \mathcal{B}_\varepsilon(\xi_{\mathbb{Z}}(s_{\mathbb{Z}}, N))$. Define $y_{\mathbb{Z}} = \mathcal{F}(x_{\mathbb{Z}})$, i.e. $y_n = f(x_n) = x_{n+1}$ for $n \in \mathbb{Z}$ and as a consequence, $y_{\mathbb{Z}} \in \mathcal{B}_\varepsilon(\xi_{\mathbb{Z}}(\sigma(s_{\mathbb{Z}}), N))$. The uniqueness property from Theorem 7 yields the asserted conjugacy $h(\sigma(s_{\mathbb{Z}})) = y_{\mathbb{Z}} = \mathcal{F}(x_{\mathbb{Z}}) = \mathcal{F}(h(s_{\mathbb{Z}}))$. ∎

5.2   Conjugacy between shift-dynamics and the dynamics on $\text{Orb}(\mathcal{O})$

For sufficiently small ε and sufficiently large N, we construct an open set $\mathcal{O}$, such that $\text{Orb}(\mathcal{O})$ coincides with $\mathcal{X}(N, \varepsilon)$. Using this result and Theorem 11, the proof of the conjugacy, described in diagram (5), is complete.

Theorem 12 *Assume **(A1)–(A4)**. Then there exist constants $\varepsilon > 0$, $N > 0$ and an open set $\mathcal{O}$, which is a neighborhood of the homoclinic orbit, such that $\text{Orb}(\mathcal{O}) = \mathcal{X}(N, \varepsilon)$.*

Proof: *Step 1: Choice of constants.* Let $\bar{\varepsilon} = \varepsilon_{\text{sol}}$ be defined as in Theorem 7. Choose $\bar{N} + 1 \ge N_{\varepsilon_{\text{sol}}}$ such that

$$\mathcal{B}_{\bar{\varepsilon}/2}(\bar{x}_{a(\bar{N}+1)+i}) \subset \mathcal{B}_{\bar{\varepsilon}}(\xi) \quad \text{for all} \quad i \le 0, i \ge \bar{N} + 1,$$

cf. Lemma 2 (i). We define

$$p(\bar{N}) := \begin{cases} \bar{N}, & \text{if } \bar{x}_{a(\bar{N}+1)+\bar{N}} \ne \xi, \\ k, & \text{if } \bar{x}_{a(\bar{N}+1)+k} \ne \xi, \bar{x}_{a(\bar{N}+1)+k+1} = \xi, \end{cases}$$

where the latter case accounts for possible snap-back behavior. Next, fix $\varepsilon \le \frac{\bar{\varepsilon}}{2}$ such that

$$\|\bar{x}_{a(\bar{N}+1)+n} - \bar{x}_{a(\bar{N}+1)+m}\| > 2\varepsilon \quad \text{for all} \quad \begin{cases} n \ne m, \ n, m \in [1, p(\bar{N})], \\ n \in [1, p(\bar{N})], \ m \notin [1, p(\bar{N})] \end{cases}$$

and

$$f\left(\bigcup_{i\leq 0,\bar{N}+1\leq i}\mathcal{B}_\varepsilon(\bar{x}_{a(\bar{N}+1)+i})\cup\mathcal{B}_\varepsilon(\xi)\right)\cap\mathcal{B}_\varepsilon(\bar{x}_{a(\bar{N}+1)+j})=\emptyset\quad\text{for all }j=2,\ldots,p(\bar{N}).\quad(43)$$

For this choice of $\varepsilon>0$, we find an $N\geq\max\{\bar{N}+2,N_\varepsilon\}$ with N_ε from Theorem 7, such that $[a(\bar{N}+1)+1,a(\bar{N}+1)+\bar{N}]\subset[a(N)+1,a(N)+N-1]$, cf. Lemma 2 (ii).

Finally, we set $\ell=a(\bar{N}+1)-a(N)$, $M:=N-p(\bar{N})$ and note $\ell\leq M-1$.

Step 2: Construction of $\mathcal{O}$. This construction is similar to the approach in [42, Theorem 5.1].

We define

$$B_0:=\bigcup_{i\leq 0,\bar{N}+1\leq i}\mathcal{B}_\varepsilon(\bar{x}_{a(\bar{N}+1)+i})\cup\mathcal{B}_\varepsilon(\xi),\quad B_i:=\mathcal{B}_\varepsilon(\bar{x}_{a(\bar{N}+1)+i})\text{ for }i=1,\ldots,p(\bar{N}),\quad(44)$$

and note that $B_0\subset\mathcal{B}_{\bar{\varepsilon}}(\xi)$.

We have to ensure that orbits in the union of these sets enter B_0 only via $B_{p(\bar{N})}$, then stay in B_0 for at least M steps. Orbits are only allowed to leave B_0 via B_1 and the i-th iterate of an orbit point in B_1 lies in B_{i+1} for $i=1,\ldots,p(\bar{N})-1$. This behavior can be achieved by further shrinking the neighborhoods.

Let $\mathcal{O}=\bigcup_{i=0}^{p(\bar{N})}V_i$, where

$$V_0:=B_0,\quad V_{p(\bar{N})}:=B_{p(\bar{N})}\cap\bigcap_{n=1}^M f^{-n}(V_0),\quad V_i:=B_i\cap f^{-1}(V_{i+1}),\ i=p(\bar{N})-1,\ldots,1.\quad(45)$$

The setting (45) and condition (43) guarantee the properties

$$x\in V_0,\ f(x)\notin V_0\ \Rightarrow\ f(x)\in V_1,$$
$$x\in V_i\ \Rightarrow\ f(x)\in V_{i+1}\quad\text{for }i=1,\ldots,p(\bar{N})-1,$$
$$x\in V_{p(\bar{N})}\ \Rightarrow\ f^n(x)\in V_0\quad\text{for }n=1,\ldots,M.$$

Step 3: $\mathcal{X}(N,\varepsilon)\supset\mathrm{Orb}(\mathcal{O})$. For $x_\mathbb{Z}\in\mathrm{Orb}(\mathcal{O})$, we introduce two sequences of symbols in $\Sigma_{A(\bar{N}+1)}^{\mathbb{Z}}$ and $\Sigma_{A(N)}^{\mathbb{Z}}$, respectively. Starting with $\Sigma_{A(\bar{N}+1)}^{\mathbb{Z}}$, we define for $n\in\mathbb{Z}$

$$\bar{s}_n:=\begin{cases}i,&\text{if }x_n\in V_i,\\p(\bar{N})+j,&\text{if }j\in[1,\bar{N}-p(\bar{N})]\text{ such that }x_{n-j}\in V_{p(\bar{N})}.\end{cases}$$

This sequence is extended to $N>\bar{N}+1$ symbols as follows, see Table 1 for an illustration:

$$s_n:=\begin{cases}\ell+i,&\text{if }\exists i\in[1,\bar{N}]:\bar{s}_n=i,\\\ell+1-i,&\text{if }\exists i\in[1,\ell+1]:\bar{s}_{n+j}=0\ \forall j\in[0,i-1]\wedge\bar{s}_{n+i}=1,\\\ell+\bar{N}+i,&\text{if }\exists i\in[1,M-\ell-1]:\bar{s}_{n-j}=0\ \forall j\in[0,i-1]\wedge\bar{s}_{n-i}=\bar{N},\\0,&\text{otherwise.}\end{cases}$$

By Theorem 7 there exists a unique $\bar{y}_\mathbb{Z}\in\mathcal{B}_{\bar{\varepsilon}}(\xi_\mathbb{Z}(\bar{s}_\mathbb{Z},\bar{N}+1))$, satisfying $\Gamma_\mathbb{Z}(\bar{y}_\mathbb{Z})=0$, and there is a second unique orbit $y_\mathbb{Z}\in\mathcal{B}_\varepsilon(\xi_\mathbb{Z}(s_\mathbb{Z},N))$, satisfying $\Gamma_\mathbb{Z}(y_\mathbb{Z})=0$. Since

$\bar{s}_\mathbb{Z}$	0	0	...	0	0	1	...	$\bar{N}$	0	...	0
$s_\mathbb{Z}$	0	1	...	$\ell-1$	ℓ	$\ell+1$	...	$\ell+\bar{N}$	$\ell+\bar{N}+1$	...	$N-1$

Table 1: Connection between symbolic sequences.

$\mathcal{B}_\varepsilon(\xi_\mathbb{Z}(s_\mathbb{Z}, N)) \subset \mathcal{B}_{\bar{\varepsilon}}(\xi_\mathbb{Z}(\bar{s}_\mathbb{Z}, \bar{N}+1))$ holds true, the uniqueness of the above orbits yields $y_\mathbb{Z} = \bar{y}_\mathbb{Z}$. Observe that $x_\mathbb{Z} \in \mathcal{B}_{\bar{\varepsilon}}(\xi_\mathbb{Z}(\bar{s}_\mathbb{Z}, \bar{N}+1))$ with $\Gamma_\mathbb{Z}(x_\mathbb{Z}) = 0$. Consequently, by the uniqueness above, $x_\mathbb{Z} = \bar{y}_\mathbb{Z} = y_\mathbb{Z} \in \mathcal{X}(N, \varepsilon)$.

Step 4: $\mathcal{X}(N, \varepsilon) \subset \mathrm{Orb}(\mathcal{O})$. For any $x_\mathbb{Z} \in \mathcal{X}(N, \varepsilon)$ there exists a unique $s_\mathbb{Z} \in \Sigma_{A(N)}^\mathbb{Z}$ such that $x_\mathbb{Z} \in \mathcal{B}_\varepsilon(\xi_\mathbb{Z}(s_\mathbb{Z}, N))$ and $\Gamma_\mathbb{Z}(x_\mathbb{Z}) = 0$ holds true. Using the construction of $\mathcal{O}$, we prove that $x_n \in \mathcal{O}$ for all $n \in \mathbb{Z}$ and thus, $x_\mathbb{Z} \in \mathrm{Orb}(\mathcal{O})$, as follows.

For $x_n \notin \bigcup_{i=1}^{p(\bar{N})} B_i$ we get $x_n \in B_0 \subset \mathcal{O}$.

For $x_n \in B_{p(\bar{N})}$ the construction (44) and $x_\mathbb{Z} \in \mathcal{X}(N, \varepsilon)$ show $f^i(x_n) \in B_0$ for all $i = 1, \ldots, M$. Thus, $x_n \in B_{p(\bar{N})} \cap \bigcap_{i=1}^M f^{-i}(V_0) = V_{p(\bar{N})} \subset \mathcal{O}$.

For $x_n \in B_i$, $i = p(\bar{N}) - 1, \ldots, 1$, we get $f(x_n) \in V_{i+1}$ by induction, from which we deduce $x_n \in B_i \cap f^{-1}(V_{i+1}) = V_i \subset \mathcal{O}$. ∎

5.3 A Homoclinic Theorem for finite orbits

In the section we provide the theorem underlying the conjugacy in the diagram (8). In a first step, replacing $\mathbb{Z}$ by J in the proof of Theorem 12 and carefully handling the boundary condition, we obtain the following finite time analog of Theorem 12.

Theorem 13 *Assume **(A1)–(A5)**. Then there exist constants $\varepsilon_\mathcal{X} > 0$, $N_\mathcal{X} > 0$ and an open set $\mathcal{O}$, which is a neighborhood of the homoclinic orbit, such that for all intervals J with $|J| \geq N_\mathcal{X} + 1$, it holds that $\mathrm{Orb}(J, \mathcal{O}) = \mathcal{X}_J(N_\mathcal{X}, \varepsilon_\mathcal{X})$.*

Recall from (10) and (9) the finite time versions $\mathcal{F}_J, \sigma_J$ of the operator $\mathcal{F}$ and the time shift σ. With these notions the finite time analog of the Homoclinic Theorem, indicated by the diagram (8), reads as follows.

Theorem 14 *Assume **(A1)–(A5)** and let $\varepsilon_\mathcal{X}$ and $N_\mathcal{X}$ be as in Theorem 13. Then for any interval $|J| \geq N_\mathcal{X} + 1$ there exists a homeomorphism $h_J : \Sigma_{A(N)}^J \to \mathrm{Orb}(J, \mathcal{O})$ such that the diagram (8) commutes, i.e. $\mathcal{F}_J \circ h_J = h_{J-1} \circ \sigma_J$.*

Proof: *Step 1: Definition of h_J.* Let J be a finite interval, satisfying $|J| \geq N_\mathcal{X} + 1$. Due to Theorem 7, for any $s_J \in \Sigma_{A(N_\mathcal{X})}^J$, there exists a unique $x_J(s_J) \in \mathcal{B}_{\varepsilon_\mathcal{X}}(\xi_J(s_J, N_\mathcal{X}))$ such that $\Gamma_J(x_J(s_J)) = 0$. Thus we conclude that $x_J(s_J) \in \mathcal{X}_J(N_\mathcal{X}, \varepsilon_\mathcal{X})$ and consequently $x_J(s_J) \in \mathrm{Orb}(J, \mathcal{O})$ by Theorem 13. We define $h_J(s_J) := x_J(s_J)$.

Step 2: h_J is a homeomorphism. For any $x_J \in \mathrm{Orb}(J, \mathcal{O}) = \mathcal{X}_J(N_\mathcal{X}, \varepsilon_\mathcal{X})$, there exists – due to Theorem 7 – a unique $s_J \in \Sigma_{A(N_\mathcal{X})}^J$ such that $x_J \in \mathcal{B}_{\varepsilon_\mathcal{X}}(\xi_J(s_J, N_\mathcal{X}))$. Since $h_J(s_J) = x_J$, we conclude that h_J is invertible. Note that $\Sigma_{A(N_\mathcal{X})}^J$ and $\mathrm{Orb}(J, \mathcal{O})$ are finite sets with the same cardinality. Hence, h_J is a homeomorphism.

Step 3: Proof of conjugacy. For any symbolic sequence $s_J \in \Sigma_{A(N_\mathcal{X})}^J$, we get $x_J = h_J(s_J) \in \mathcal{B}_{\varepsilon_\mathcal{X}}(\xi_J(s_J, N_\mathcal{X}))$. Let $y_{J-1} = \mathcal{F}_J(x_J)$, then it follows that $y_n = x_{n+1}$ for all

$n \in J - 1$. As a consequence, $y_{J-1} \in \mathcal{B}_{\varepsilon_{\mathcal{X}}}(\xi_{J-1}(\sigma_J(s_J), N_{\mathcal{X}}))$ and $\Gamma_{J-1}(y_{J-1}) = 0$. From this, we deduce $h_{J-1}(\sigma_J(s_J)) = y_{J-1} = \mathcal{F}_J(h_J(s_J))$. ∎

6 Computation and visualization of the maximal invariant set and its coding

In this section, we illustrate the theory by applying the algorithm from Section 2.2 to several examples. In each case we approximate the maximal invariant set $\mathcal{O}_c$, defined in (13), by solving appropriate boundary value problems, and we indicate the symbolic coding for points close to the midpoint of the primary homoclinic orbit.

First, we comment on how to verify our hyperbolicity assumptions.

6.1 Transversality of homoclinic orbits from a geometric point of view

Unlike in the invertible case, stable and unstable sets of a fixed point ξ are in general not immersed submanifolds of $\mathbb{R}^d$. Nevertheless, these sets have graph representations near the fixed point, cf. [12, Theorem 3.1], [42, Theorem 4.1]:

$$W_{\text{loc}}^s(\xi) = \{\xi + x_s + h_s(x_s) : x_s \in U_s\}, \quad W_{\text{loc}}^u(\xi) = \{\xi + x_u + h_u(x_u) : x_u \in U_u\},$$

where $h_{s,u} : U_{s,u} \to U_{u,s}$ is smooth and $U_{s,u}$ denote sufficiently small neighborhoods of 0 within the stable and unstable subspace of $Df(\xi)$, respectively. Note that the global stable set can be obtained by continuation in backward time in a set valued sense, while the stable set is obtained by iterating in forward time. One can verify transversality of the homoclinic orbit $\bar{x}_{\mathbb{Z}}$, i.e. an exponential dichotomy of the variational equation (1) with projectors $\bar{P}_n^{s,u}$, $n \in \mathbb{Z}$, if the following conditions are satisfied, see [42, Theorem 4.2]:

$$Df^{n-m}(\bar{x}_m) T_{\bar{x}_m} W_{\text{loc}}^u(\xi) \oplus T_{\bar{x}_n} W_{\text{loc}}^s(\xi) = \mathbb{R}^d, \quad Df^{n-m}(\bar{x}_m)_{|T_{\bar{x}_m} W_{\text{loc}}^u(\xi)} \text{ is invertible}$$

with

$$T_{\bar{x}_m} W_{\text{loc}}^u(\xi) = \mathcal{R}(\bar{P}_m^u), \quad T_{\bar{x}_n} W_{\text{loc}}^s(\xi) = \mathcal{R}(\bar{P}_n^s) \tag{46}$$

for all $m \leq -N_{\text{loc}}$ and all $n \geq N_{\text{loc}}$ and a suitable $N_{\text{loc}} \in \mathbb{N}$. We refer to [32, Proposition 5.4] and [18, Theorem 3.5] for corresponding results for invertible systems in the autonomous as well as the nonautonomous case.

Assume that the variational equation (1) has an exponential dichotomy and let Φ denote its solution operator, then

$$\mathcal{R}(\bar{P}_n^s) = \{u \in \mathbb{R}^d : \sup_{k \geq n} \|\Phi(k, n)u\| < \infty\}, \tag{47}$$

see [3, Theorem 2.5]. For a general point $x \in W^{s,u}(\xi)$, we define the stable and unstable tangent set:

$$T_x W^{s,u}(\xi) = \{v \in \mathbb{R}^d : \exists \zeta \in \mathcal{C}^1((-\varepsilon, \varepsilon), W^{s,u}(\xi)) : \zeta(0) = x, \ \zeta'(0) = v\}.$$

Lemma 15 *Assume **(A1)**–**(A4)**. Then the following assertions hold for all $n \in \mathbb{Z}$:*

(i) $\mathcal{R}(\bar{P}_n^u) \subset T_{\bar{x}_n} W^u(\xi)$,

(ii) $\mathcal{N}(Df(\bar{x}_n)) \subset \mathcal{R}(\bar{P}_n^s)$.

Proof:

(i) Fix $n \in \mathbb{Z}$. For $n \leq -N_{\mathrm{loc}}$, the assertion follows from (46).
For $n > -N_{\mathrm{loc}}$, observe that $f^{n+N_{\mathrm{loc}}}(\bar{x}_{-N_{\mathrm{loc}}}) = \bar{x}_n$ and since f is noninvertible in general, we conclude that $f^{-n-N_{\mathrm{loc}}}(\bar{x}_n) \supset \{\bar{x}_{-N_{\mathrm{loc}}}\}$ in a set valued sense. As a consequence, we obtain

$$\mathcal{R}(\bar{P}_n^u) = Df^{n+N_{\mathrm{loc}}}(\bar{x}_{-N_{\mathrm{loc}}}) \mathcal{R}(\bar{P}_{-N_{\mathrm{loc}}}^u) = Df^{n+N_{\mathrm{loc}}}(\bar{x}_{-N_{\mathrm{loc}}}) T_{\bar{x}_{-N_{\mathrm{loc}}}} W_{\mathrm{loc}}^u(\xi)$$
$$\subset T_{\bar{x}_n} W^u(\xi).$$

(ii) For $v \in \mathcal{N}(Df(\bar{x}_n))$, we conclude that $\Phi(k,n)v = Df^{k-n}(\bar{x}_n)v = 0$ for all $k \geq n+1$. Using (47), we immediately get $v \in \mathcal{R}(\bar{P}_n^s)$.

∎

We apply this lemma in Section 6.6 and illustrate that the given model from mathematical finance has an exponential dichotomy for one set of parameters, while the regularity condition (ii) in Definition 18 is violated for a second set of parameters.

The examples that we analyze in the following sections show different characteristics, concerning their invertibility:

Sect. 6.2: An invertible system with identical stable and unstable dichotomy rates.

Sect. 6.3: An invertible three-dimensional map with a two-dimensional stable manifold.

Sect. 6.4: A model for which $Df(\bar{x}_n)$ is noninvertible for all $n \in \mathbb{Z}$.

Sect. 6.5: A map – showing wild chaos – that is noninvertible but still locally invertible near each finite $x \in \mathbb{R}^2 \setminus \{0\}$.

Sect. 6.6: A model from mathematical finance for which $Df(\bar{x}_n)$ is noninvertible for exactly one $n \in \mathbb{Z}$.

6.2 The invertible Hénon map

Our first example is the well known Hénon map that plays the role of a normal form for invertible, quadratic, two-dimensional maps, see [13]:

$$F \begin{pmatrix} x_1 \\ x_2 \end{pmatrix} = \begin{pmatrix} 1 + x_2 - ax_1^2 \\ bx_1 \end{pmatrix}. \tag{48}$$

A generalized version of the Hénon map possessing nontrivial orientation properties has been studied in [11] and [9].

We consider here the parameters $a = 1.4$, $b = -1$ for which the Hénon map (48) is orientation preserving and possesses two primary homoclinic orbits. As in steps (Ia), (Ib) of the algorithm, these are determined via parameter continuation. The resulting orbits
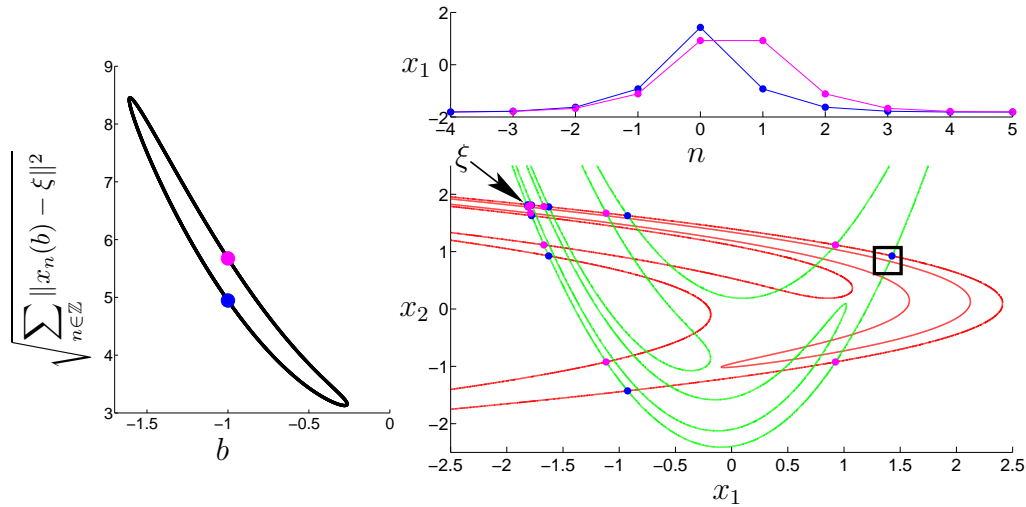
Figure 4: Two homoclinic orbits (blue and magenta in the upper right picture) of (48), found via numerical continuation w.r.t. the parameter b (left diagram). The lower right figure additionally shows stable (green) and unstable (red) manifolds of the fixed point ξ. A zoom of the black square is given in Figure 5.

are depicted in Figure 4 together with a continuation diagram. The variational equations (1) along these homoclinic orbits turn out to have exponential dichotomies with identical rates $\bar{\alpha}_s = \bar{\alpha}_u \approx 1.58$.

Next, we execute steps (II)-(V) of our algorithm and obtain Figure 5, which reveals the local structure of the maximal invariant set by zooming into the black square of Figure 4. In our diagrams we will display the coding of the computed homoclinic points by a shorter sequence $s_{[k_-,k_+]} \in \Sigma_{A(1^\ell)}$. Due to the construction in step (II) of the algorithm, the symbolic sequence $s_{[k_-,k_+]}$ satisfies condition (15), which allows a shorter coding, realized by colored tuples. We explain the coding by taking the example from Figure 1. Take the sequence in $\Sigma_{A(1^2)}$

$$\cdots \quad 0 \quad 1 \quad 0 \quad 0 \quad 0 \quad 0 \quad \mathbf{1} \quad 0 \quad 0 \quad 0 \quad 2 \quad 0 \quad \cdots$$

where the $\mathbf{1}$ denotes the center element at position 0. We count the zero symbols on the left and right of the center element and introduce the coding $(4,3)$. The blue color of 4 symbolizes that the orbit on the left is of type 1, while the magenta color of 3 indicates an orbit of type 2 on the right.

Figure 5, shows the gain in information when passing over from $\ell = 1$ primary homoclinic orbit (left diagram) to $\ell = 2$ orbits (right diagram). Note that points with the coding $(1,i)$, $i \in \{1,\ldots,10\}$ lie outside the plotting area of Figure 5 (right).

We now consider three-humped orbits of type $\ell = 1$ and derive an estimate between certain points in the maximal invariant set. For $N \geq N_{\text{sol}}$ let $z_{\mathbb{Z}}^{1,2}$ be two homoclinic orbits, coded by (i,k) and (j,k), respectively. The left diagram in Figure 5 shows a small common neighborhood of $z_{\bar{n}}^{1,2}$ for $\bar{n} = 0$.
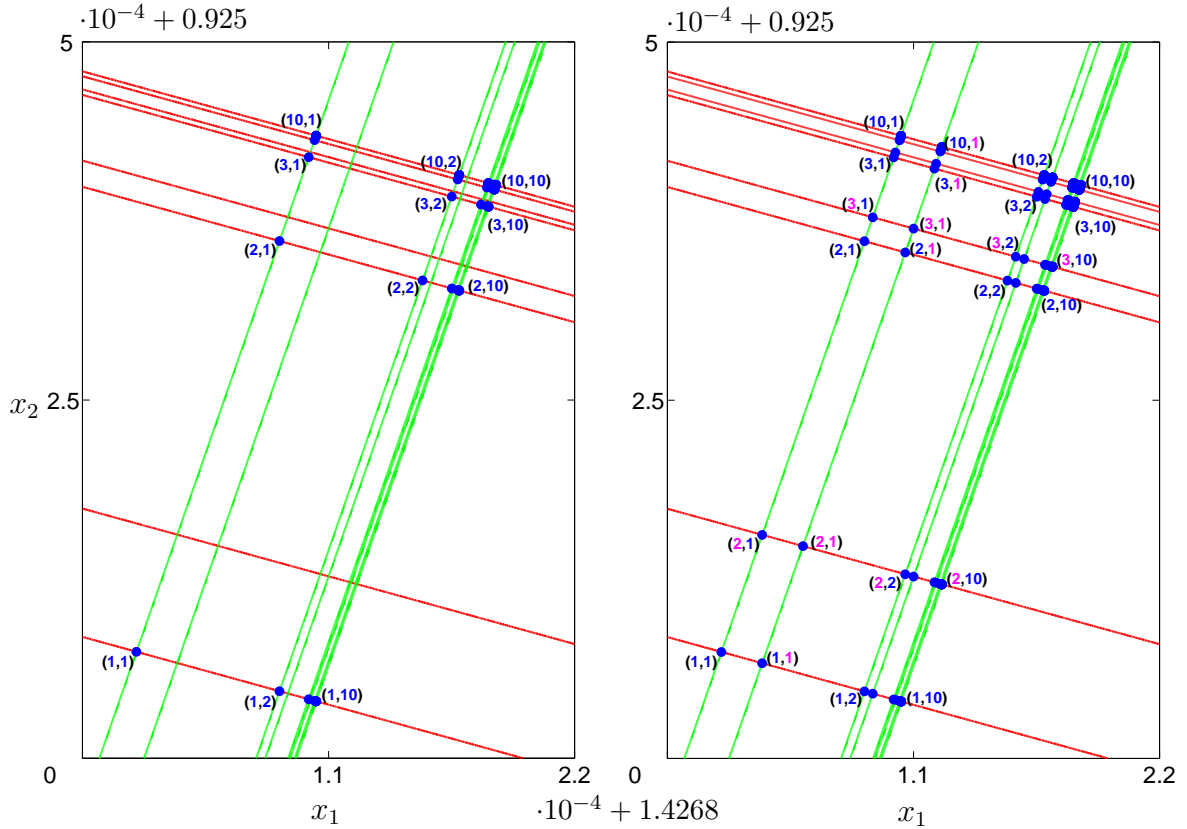
28

Figure 5: Zoom of the black square from Figure 4. Points in the maximal invariant set are computed by the algorithm from Section 2.2 with $J = [-3, 3]$, $-k_- = k_+ = 10$. Humps of $\ell = 1$ type only (left) and of both types (right). Note that the distance between points of type $(i, k), (j, k)$ (resp. $(k, i), (k, j)$) converges to zero as k increases, cf. (49), (50) resp.

Denote by $\tilde{s}_{\mathbb{Z}}^{1,2}$ the corresponding coding in $\Sigma_{A(1^1)}$ and let $s_{\mathbb{Z}}^{1,2} := g(\tilde{s}_{\mathbb{Z}}^{1,2}, 1)$ be the coding in $\Sigma_{A(N)}^{\mathbb{Z}}$, where g is defined in (14).

Since the second symbols in the short coding coincide, we conclude $s_n^1 = s_n^2$ for $n \geq m_- := \max\{-i, -j\} + 1$. Using Theorem 8 on the interval $[m_-, m_+]$ (which applies for sufficiently large m_+), we get in the limit $m_+ \to \infty$ for $\bar{n} \geq m_-$

$$\|z_{\bar{n}}^1 - z_{\bar{n}}^2\| \leq L\varepsilon_{\text{sol}} e^{-\beta_s(\bar{n} - m_-)}. \tag{49}$$

Thus, the distance between these points essentially depends on the stable dichotomy rate. Note that this result also holds true for finite time computations, see Corollary 9. Furthermore, our numerical experiments suggest that corresponding points of these orbits lie on the same segment of the stable manifold.

If we consider coding symbols (k, i) and (k, j) with identical first entries, then *stable* has to be replaced by *unstable* in the discussion from above. The corresponding estimate from Theorem 8 reads with $m_+ := \min\{i, j\} + N - 2$ and $\bar{n} \leq m_+$:

$$\|z_{\bar{n}}^1 - z_{\bar{n}}^2\| \leq L\varepsilon_{\text{sol}} e^{-\beta_u(m_+ - \bar{n})}. \tag{50}$$

6.3 A three-dimensional invertible Hénon map

We demonstrate in this section that our algorithm from Section 2.2 can easily be applied to higher-dimensional systems. In contrast to the two-dimensional case, a meaningful presentation of the numerical output turns out to be an additional challenge. We meet this challenge, using the contour algorithm, see [20, Section 4], that allows to approximate two-dimensional invariant manifolds in three-dimensional discrete time systems.

Consider a three-dimensional version of Hénon's map proposed in [7, Example 2]:

$$F \begin{pmatrix} x_1 \\ x_2 \\ x_3 \end{pmatrix} = \begin{pmatrix} a + bx_3 - x_1^2 \\ x_1 \\ x_2 \end{pmatrix} \quad \text{with} \quad a = 1.4, \ b = 0.3. \tag{51}$$

First, we compute a homoclinic orbit w.r.t. the fixed point ξ, where

$$\xi_i = \frac{b-1}{2} + \sqrt{\frac{(b-1)^2}{4} + a}, \quad i = 1, 2, 3.$$

The matrix $DF(\xi)$ has one unstable and two stable eigenvalues and consequently, the stable manifold is two-dimensional, while the unstable manifold in of dimension one.

In a second step, we apply numerical continuation w.r.t. the parameter b, resulting in the closed loop of homoclinic orbits, shown in the left diagram in Figure 6. The right diagram displays the x_1-components of the corresponding orbits for $b = 0.3$. Note that (51) implies that the other two components are time-shifted versions of the first one, i.e. the x_1-component at time n equals the x_2-component at time $n+1$ and the x_3-component at time $n+2$. A phase-plot of these orbits together with approximations of stable and unstable manifolds is given in Figure 7.
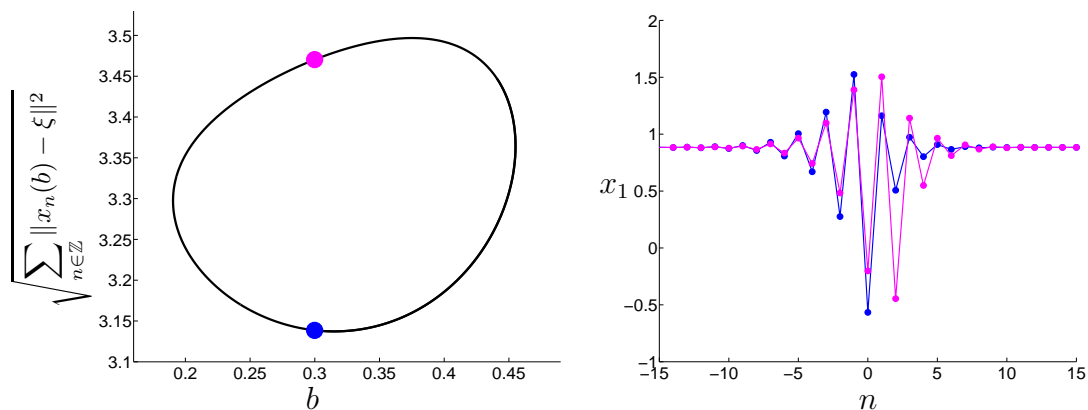

Figure 6: Continuation of homoclinic orbits of (51) w.r.t. b (left). The right diagram shows two orbits for $b = 0.3$.

An analysis of the local structure of the maximal invariant set inside the black box in Figure 7 is carried out as described in the previous section. Figure 8 illustrates the output of this procedure.
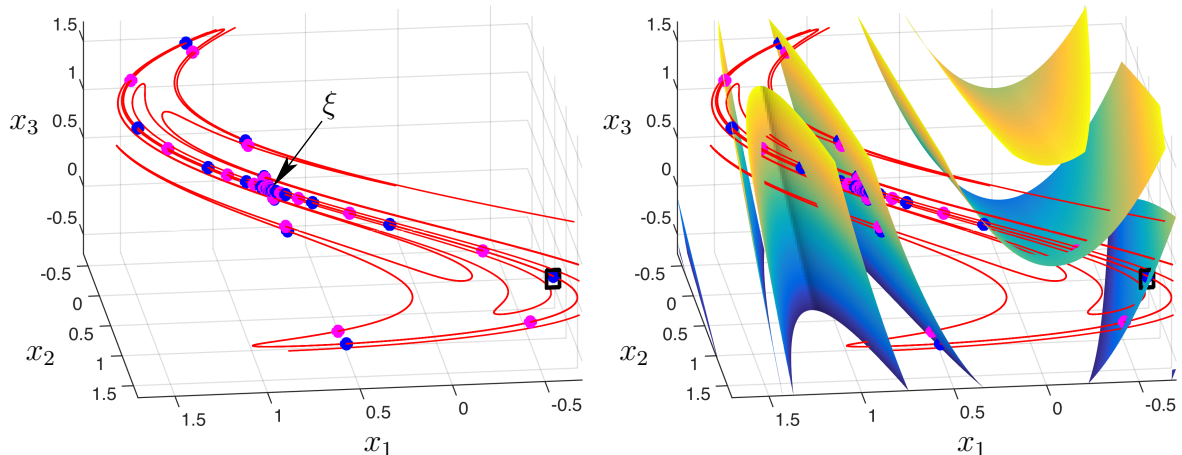
Figure 7: The two homoclinic orbits from Figure 6, shown with the unstable manifold of ξ in red (left panel) and with parts of the two-dimensional stable manifold (right panel). A zoom of the small black box in the right panel is provided in Figure 8.

6.4 A noninvertible Hénon example

Denote by $\xi \approx (-1.82, 1.82)$ a fixed point of (48) with stable and unstable eigenvalues and vectors

$$DF(\xi)x_s = \lambda_s x_s, \quad DF(\xi)x_u = \lambda_u x_u$$

and let $\mathcal{V}^{s,u}$ be the corresponding stable and unstable subspaces. We modify this system such that the stable eigenvalue is 0 while the unstable eigenvalue is unchanged. In this way, we create the noninvertible system

$$G(x) := F(x) + A \cdot (F(x) - \xi), \quad \text{where} \quad A := \begin{pmatrix} -x_s & 0 \end{pmatrix} \cdot \begin{pmatrix} x_s & x_u \end{pmatrix}^{-1}. \tag{52}$$

It turns out that dynamics are reduced to a one-dimensional line $\mathcal{D} := \mathcal{V}^u + \xi$.

Lemma 16 *For each $x \in \mathbb{R}^2$ we get $G(x) \in \mathcal{D}$.*

Proof: For $x \in \mathbb{R}^2$ let $y = x - \xi$. It follows that

$$
\begin{aligned}
G(x) &= G(\xi + y) = F(\xi + y) + A \cdot (F(\xi + y) - \xi) \\
&= (I + A)\left(F(\xi) + \int_0^1 DF(\xi + \tau y)d\tau \cdot y\right) - A\xi \\
&= \xi + (I + A)(z_s + z_u) = \xi + z_s + z_u - z_s = \xi + z_u,
\end{aligned}
$$

where $z = \int_0^1 DF(\xi + \tau y)d\tau \cdot y$, $z_{s,u} = z_{|\mathcal{V}^{s,u}}$. ∎

As a consequence, it suffices to analyze the one-dimensional reduced system, defined as

$$\lambda \mapsto \mu(\lambda), \quad \text{where} \quad G(\xi + \lambda x_u) = \xi + \mu(\lambda)x_u. \tag{53}$$

Figure 9 shows the two-dimensional systems (52) together with a homoclinic orbit as well as stable and unstable manifolds of ξ. The right diagram illustrates corresponding data
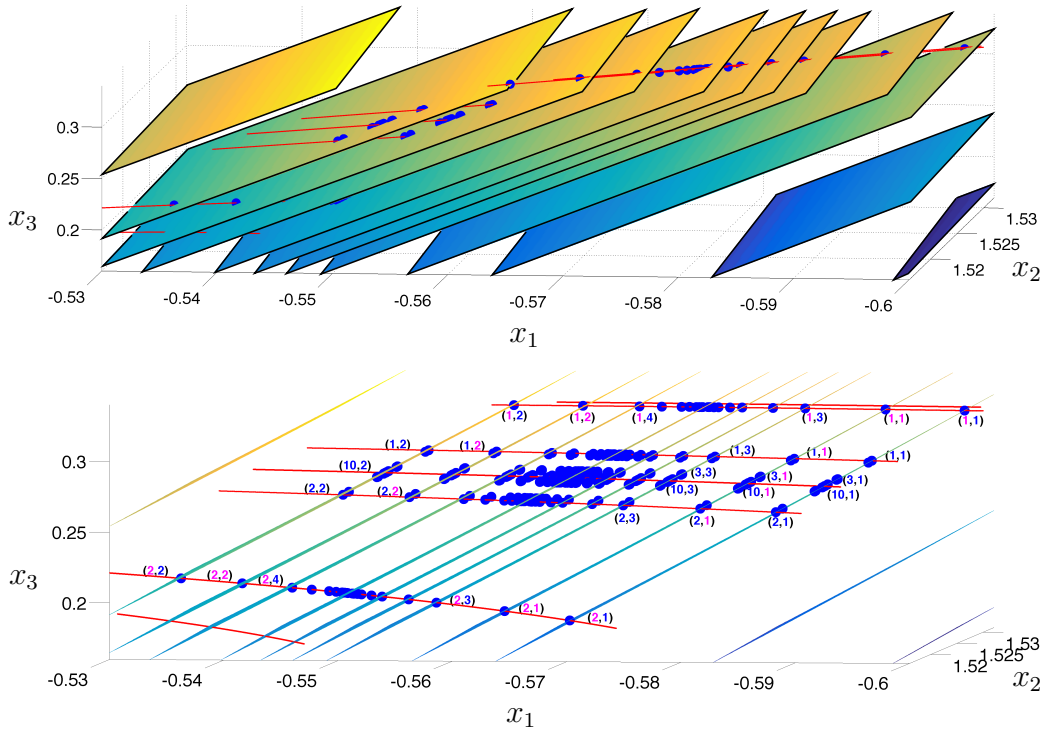
Figure 8: Zoom of the black box from Figure 7. Points in the maximal invariant set are computed by the algorithm from Section 2.2 with $J = [-4, 4]$, $-k_- = k_+ = 10$. The upper diagram shows the (visible) computed points and parts of the one-dimensional unstable manifold (red) and of the two-dimensional stable manifold of ξ. The lower diagram appears when slightly rotating the upper one such that the leaves almost collapse to lines. In the latter figure we also illustrate the coding of the homoclinic points.

for the reduced system. It turns out that the variational equation along the homoclinic orbit in the full system (52) has an exponential dichotomy, where the range of the unstable projector P_n^u satisfies $\mathcal{R}(P_n^u) = \mathcal{V}^u$ for all $n \in \mathbb{Z}$.

Note that the fixed point 0 in the reduced system (53) is unstable and has two pre-images. Thus, homoclinic orbits may exist and in this case, the unstable fixed point is called a snap-back repeller in the literature. One of the first proofs of chaos (in the sense of Li and Yorke, cf. [4, Def. 3.1]) in this noninvertible context is due to Marotto, see [26] and ensuing literature.

In Figure 10, we apply the algorithm from Section 2.2 to compute points in the intersection of the maximal invariant set with the black box from Figure 9. The zoom in Figure 10 illustrates the fractal structure of the maximal invariant set.

For $k \in \mathbb{N}$ the set of tuples $(\cdot, k) := \{(i, k) : i \in \mathbb{N}\}$ symbolizes the coding of corresponding points of the homoclinic orbits. In this example, $\lambda_s = 0$ and hence, the dichotomy rate β_s can be chosen arbitrarily large. With the notation from Section 6.2, equation (49) gives $\|z_{\bar{n}}^1 - z_{\bar{n}}^2\| = 0$ for orbits $z_{\mathbb{Z}}^{1,2}$ with symbolic coding (i, k) and (j, k), respectively and $\bar{n} \geq \max\{-i, -j\} + 1$. Thus, orbit points $z_{\bar{n}}^{1,2}$, with the coding $(\cdot, k)$ coincide and our numerical approximations of these points are identical up to machine
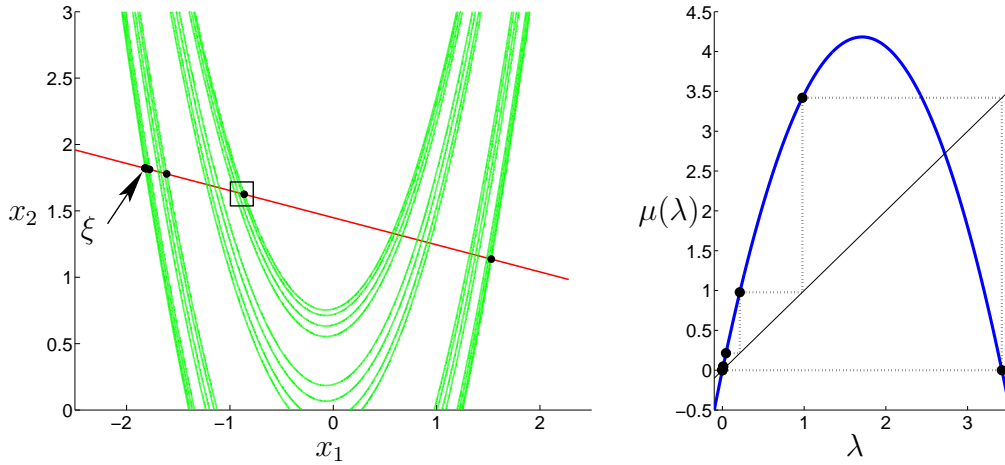
Figure 9: Left diagram: Homoclinic orbit of (52) (black points) with stable (green) and unstable (red) manifolds of the fixed point ξ. The right diagram shows the same homoclinic orbit in the reduced system (53) as well as a snap-back behavior of this orbit.

accuracy.

The maximal invariant set contains further points in the intersection of the stable and unstable manifolds. These points belong to different primary homoclinic orbits as described in Section 2.1. There is a multitude of such orbits, since each point of a homoclinic orbit has two pre-images.
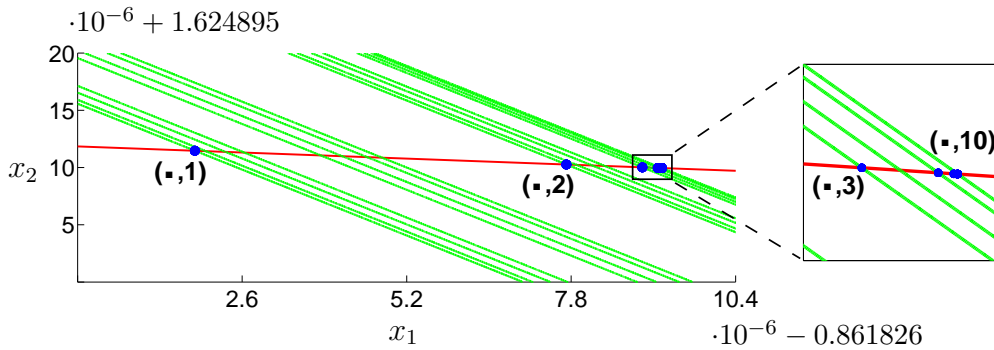
Figure 10: Maximal invariant set within the black box from Figure 9. For the computation we use $-k_- = k_+ = 10$ and $J = [-3, 4]$.

6.5 A model for wild chaos

The notion of wild chaos refers to the existence of a hyperbolic set with robust homoclinic tangencies. Wild chaos can occur in vector fields, diffeomorphism and noninvertible difference equations of at least dimension four, three and two, respectively. The model that

we analyze here originates from [5],

$$F : \mathbb{R}^2 \setminus \{0\} \rightarrow \mathbb{R}^2,$$
$$x = \begin{pmatrix} x_1 \\ x_2 \end{pmatrix} \mapsto \frac{1 - \lambda + \lambda \|x\|_2^a}{\|x\|_2^2} \begin{pmatrix} x_1^2 - x_2^2 \\ 2x_1 x_2 \end{pmatrix} + c. \tag{54}$$

The authors of [5] reduce the flow of a special vector field on the solid torus $\mathcal{T}^n$ of dimension $n \geq 5$ to the dynamics of this map. Detailed investigations of wild chaos for this map can be found in [15, 28, 16, 17]. The authors use Cl_MatContM to compute homoclinic orbits and their tangencies by solving suitable boundary value problems.

We use similar techniques but concentrate on calculating the maximal invariant set. As in [15, Figure 19 (d)], our parameters are

$$a = 0.8, \quad \lambda = 0.8, \quad c = \begin{pmatrix} 1.3 \\ 0.2 \end{pmatrix}.$$

We illustrate the maximal invariant set by computing homoclinic orbits together with stable and unstable manifolds of the fixed point.

For a more global picture, we transform the system to the square $[-1, 1]^2$ by the transformation $T(x) = \frac{x}{1 + \|x\|_\infty}$, see Figure 11. This transformation is better suited for our contour algorithm than the Poincaré disk used in [15], [16], and we accept the loss of smoothness caused by this transformation on the diagonals.
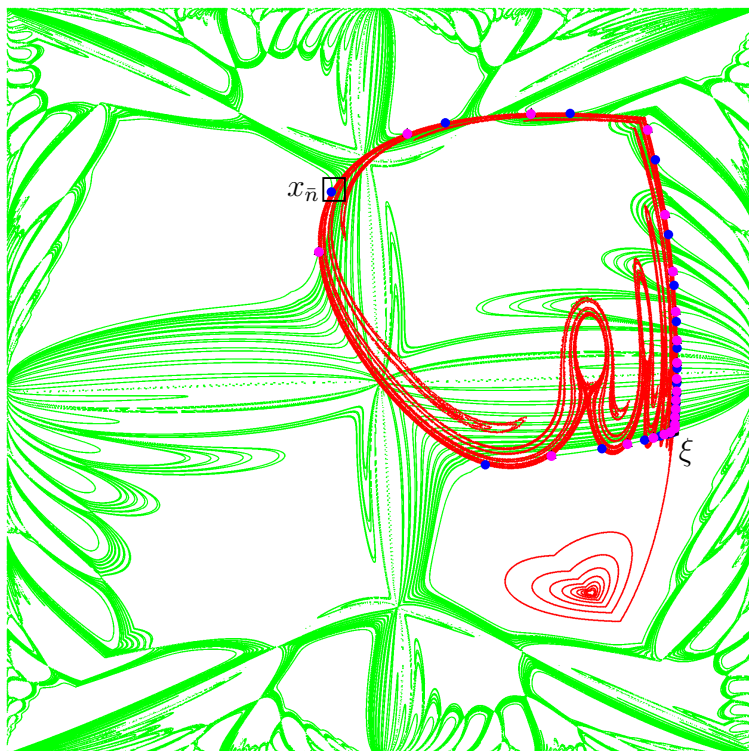

Figure 11: Two homoclinic orbits of (54) together with an approximation of the stable (green) and unstable (red) set of the fixed point ξ.

34

An illustration of the maximal invariant set within the black box in Figure 11 is given in Figure 12.
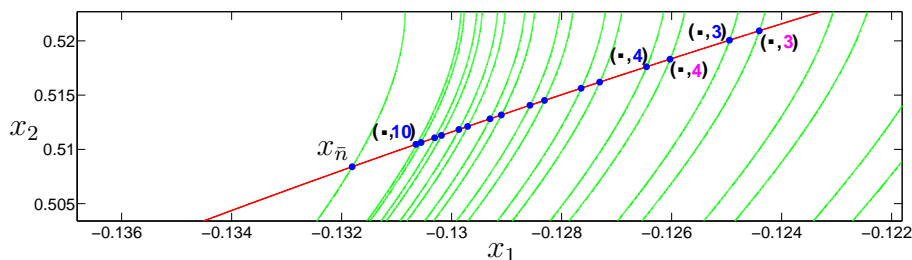

Figure 12: Maximal invariant set within the black box from Figure 11. For the computation we use $-k_- = k_+ = 10$ and $J = [-10, 9]$, $\ell = 2$.

The dichotomy rates of the variational equation along the homoclinic orbit are $\beta_s \approx 0.67$ and $\beta_u \approx 0.26$. Comparing the estimate (49) with (50), we expect – in agreement with our numerical computations – that points with coding symbols from the set $(\cdot, k) := \{(i, k) : i \in \mathbb{N}\} \cup \{(i, k) : i \in \mathbb{N}\}$, for example, are distinct, but lie in a small common neighborhood. These points cannot be distinguished within the graphical resolution of Figure 12. For details on the color coding in case of $\ell = 2$ primary humps, we refer to Section 6.2 and Figure 1.

6.6 A noninvertible model of asset pricing

The following system describes mean (x_1) and variance (x_2) of asset prices

$$F(x, \gamma) = \begin{pmatrix} x_1 \left(\delta + \frac{1-\delta}{\gamma - x_2} \right) \\ \delta x_2 + (1-\delta)x_1^2 \left(\frac{1}{\gamma - x_2} - 1 \right)^2 \end{pmatrix}, \qquad (55)$$

where the parameter $\delta = 0.8$ is fixed and the parameter γ will be varied. The underlying model, see [8, Equation (23)], is based on the interaction of two groups of investors that believe in fundamental values of an asset or in statistical data only, respectively. This model exhibits homoclinic orbits w.r.t. the fixed point $\xi = 0$, which proves chaotic dynamics in case Assumption (A4) is satisfied.

In the context of this paper, we are particularly interested in the noninvertible setup, in which a point of the homoclinic orbit lies on the critical set $\mathcal{J}_0(\gamma) = \{x \in \mathbb{R}^2 : \det(D_x F(x, \gamma)) = 0\}$, see [27, Chapter 3] for more detail on this *Ligne Critique*.

We find this codimension-one phenomenon for (55) by applying continuation techniques, cf. [1], to homoclinic orbits in combination with a bisection scheme. At the value $\bar{\gamma} \approx -0.02779678052809343$, the sets $W^s(\xi, \bar{\gamma})$, $W^u(\xi, \bar{\gamma})$ and $\mathcal{J}_0(\bar{\gamma})$ have a common point of intersection $y_{\bar{n}}$. A plot of the corresponding homoclinic orbit $y_\mathbb{Z}$ is given in the left diagram in Figure 13.

It turns out that our Assumptions (A1)–(A4) are satisfied for the parameter value $\bar{\gamma}$. Denote by $P_n^{s,u}$, $n \in \mathbb{Z}$ the dichotomy projectors of the corresponding variational equation.
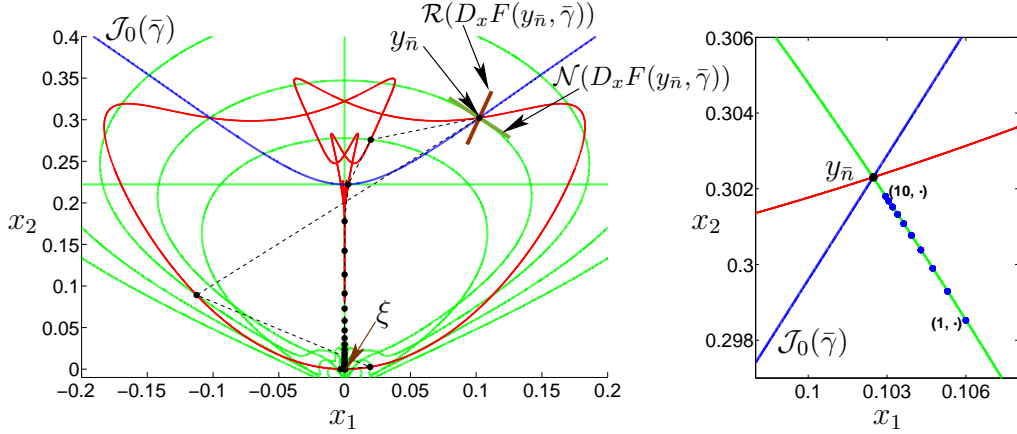
Figure 13: Left diagram: Stable (green) and unstable (red) set of the fixed point ξ together with the homoclinic orbit segment y_J, $J = [-40, 40]$ (black points). The critical curve $\mathcal{J}_0(\bar{\gamma})$ is shown in blue. At the point $y_{\bar{n}} \in \mathcal{J}_0(\bar{\gamma})$, the maximal invariant set in a neighborhood of $y_{\bar{n}}$ is depicted in the right diagram for $-k_- = k_+ = 10$ and $J = [-14, 14]$.

Lemma 15 (ii) and Lemma 17 give the following relations between dichotomy projectors and range, nullspace of $D_x F(y_{\bar{n}}, \bar{\gamma})$:

$$\begin{aligned}
\mathcal{N}(D_x F(y_{\bar{n}}, \bar{\gamma})) &\subset \mathcal{R}(P_{\bar{n}}^s), \\
\mathcal{R}(D_x F(y_{\bar{n}}, \bar{\gamma})) &= \mathcal{R}(P_{\bar{n}+1}^u) \subset T_{y_{\bar{n}+1}} W^u(\xi, \bar{\gamma}).
\end{aligned}$$

Lemma 17 *Assume that f satisfies* **(A1)**–**(A4)** *for space dimension $d = 2$. Further assume that $\dim \mathcal{R}(\bar{P}_{\bar{n}}^s) = 1$ and that $\dim \mathcal{N}(Df(\bar{x}_{\bar{n}})) = 1$.*
  Then $\mathcal{R}(Df(\bar{x}_{\bar{n}})) = \mathcal{R}(\bar{P}_{\bar{n}+1}^u) \subset T_{\bar{x}_{\bar{n}+1}} W^u(\xi)$.

Proof: If follows from **(A4)** that $Df(\bar{x}_{\bar{n}}) : \mathcal{R}(\bar{P}_{\bar{n}}^u) \to \mathcal{R}(\bar{P}_{\bar{n}+1}^u)$ is invertible. Since $\mathcal{R}(Df(\bar{x}_{\bar{n}}))$ and $\mathcal{R}(\bar{P}_{\bar{n}+1}^u)$ are one-dimensional subspaces, they coincide and the claim follows with Lemma 15 (i). ∎

The maximal invariant set in a neighborhood of $y_{\bar{n}}$ is displayed in the right panel of Figure 13. The dichotomy rates of the variational equation along the homoclinic orbit are $\beta_s \approx 0.22$ and $\beta_u \approx 1.86$. From the estimates (49) and (50), we expect – in accordance with our numerical results – that points having a symbolic coding from the set $(k, \cdot) := \{(k, i) : i \in \mathbb{N}\}$ are distinct but lie in a small common neighborhood. Note that we do not plot the unstable set passing through these points in this tiny neighborhood, since there is a lack of a fast algorithm that works accurately for this task.

Finally, we consider a second parameter value $\tilde{\gamma} \approx -0.04212651463673642$ for which the stable and unstable sets as well as $\mathcal{J}_0(\tilde{\gamma})$ also have a common point of intersection, see Figure 14. Denote by $z_{\mathbb{Z}}$ the corresponding homoclinic orbit and let $z_{\tilde{n}}$ be the point of this orbit, lying on $\mathcal{J}_0(\tilde{\gamma})$.

But now the Assumption **(A4)** is not satisfied, since the regularity condition (ii) in Definition 18 is violated. For proving this statement, assume to the contrary that the
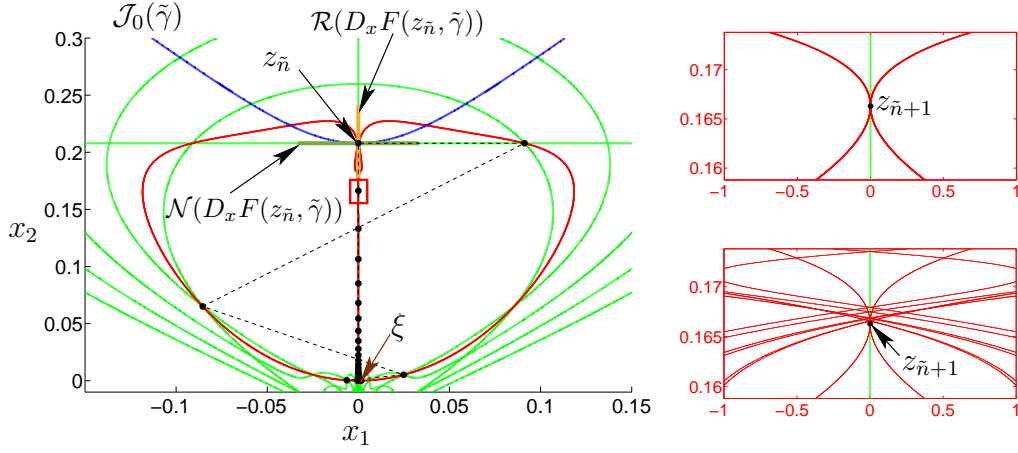
Figure 14: Left diagram: Stable (green) and unstable (red) set of the fixed point ξ together with the homoclinic orbit segment z_J, $J = [-40, 40]$ (black points). The critical curve $\mathcal{J}_0(\tilde{\gamma})$ is shown in blue. Zooms of the red box are given in the right diagrams. The upper figure illustrates tangential intersections of stable and unstable sets at the point $z_{\tilde{n}+1}$. The lower diagram shows an extensive continuation of the unstable set, indicating additional transversal intersections close to $z_{\tilde{n}+1}$, but not exactly at $z_{\tilde{n}+1}$.

variational equation has an exponential dichotomy with projectors $P_n^{s,u}$, $n \in \mathbb{Z}$. Note that

$$D_x F\left(\begin{pmatrix} 0 \\ x_2 \end{pmatrix}, \tilde{\gamma}\right) = \begin{pmatrix} \delta + \frac{1-\delta}{\tilde{\gamma} - x_2} & 0 \\ 0 & \delta \end{pmatrix}$$

and this matrix is invertible for $x_2 \neq \tilde{x}_2 := \frac{1-\delta}{\delta} + \tilde{\gamma} \approx 0.207$. It turns out that $z_{\tilde{n}} = \begin{pmatrix} 0 \\ \tilde{x}_2 \end{pmatrix}$ and consequently, $D_x F(z_\ell, \tilde{\gamma})$ is invertible for all $\ell \geq \tilde{n} + 1$. On the one hand, Lemma 17 yields $\mathcal{R}(P_{\tilde{n}+1}^u) = \mathcal{R}(D_x F(z_{\tilde{n}}, \tilde{\gamma})) = \mathcal{V}^s := \{\lambda \binom{0}{1} : \lambda \in \mathbb{R}\}$. On the other hand, $\mathcal{V}^s$ is invariant w.r.t. $\Phi(\tilde{n} + 1, \ell)$ for all $\ell \geq \tilde{n} + 1$ and we conclude with Lemma 15 (ii) that $\mathcal{R}(P_{\tilde{n}+1}^s) = \Phi(\tilde{n} + 1, \ell)\mathcal{R}(P_\ell^s) \supset \Phi(\tilde{n} + 1, \ell)\mathcal{N}(D_x F(z_{\tilde{n}}, \tilde{\gamma})) = \Phi(\tilde{n} + 1, \ell)\mathcal{V}^s = \mathcal{V}^s$ for all $\ell \geq \tilde{n} + 1$. As a consequence $\mathcal{R}(P_{\tilde{n}+1}^s) \cap \mathcal{R}(P_{\tilde{n}+1}^u) \neq \{0\}$ and thus, the variational equation cannot have an exponential dichotomy. In particular, we see for this parameter setup that our theorems do not apply.

Note that a simultaneous occurrence of transversal and tangential intersections of stable and unstable sets along the same homoclinic orbit is not generic, see the discussion in [35, Section 4].

Acknowledgment

37

A Appendix

A.1 Exponential dichotomy

In this appendix, we summarize important results from the theory of exponential dichotomies in a noninvertible setup.

Let $J = [n_-, n_+]$, $\tilde{J} = [n_-, n_+ - 1]$ where the cases $n_- = -\infty$ and $n_+ = \infty$ are permitted. Consider the nonautonomous linear difference equation

$$u_{n+1} = A_n u_n, \quad A_n \in \mathbb{R}^{d,d}, \quad n \in \tilde{J} \tag{56}$$

and denote by $\Phi(m,n) = A_{m-1} \cdots A_n, m \geq n$ its forward solution operator. We define the notion of an exponential dichotomy, see [14, Def. 7.6.1] that is called regular in [2, Def. 3.1] and [22, Def. 2.1.2].

Definition 18 *The difference equation* (56) *has an **exponential dichotomy** on J with data $(K, \alpha_{s,u}, P_n^{s,u})$, if there exist constants $K, \alpha_s, \alpha_u > 0$ and families of projectors P_n^s, $P_n^u := I - P_n^s$, $n \in J$ such that*

(i) $P_n^{s,u} \Phi(n,m) = \Phi(n,m) P_m^{s,u}$ for all $n, m \in J$, $n \geq m$,

(ii) $A_n|_{\mathcal{R}(P_n^u)} : \mathcal{R}(P_n^u) \to \mathcal{R}(P_{n+1}^u)$ is invertible for all $n \in \tilde{J}$ with the inverse of $\Phi(n,m)|_{\mathcal{R}(P_m^u)}$, $n \geq m$ denoted by $\bar{\Phi}(m,n) : \mathcal{R}(P_n^u) \to \mathcal{R}(P_m^u)$.

(iii) For $n, m \in J$, $n \geq m$ the following estimates hold:

$$\|\Phi(n,m) P_m^s\| \leq K \mathrm{e}^{-\alpha_s(n-m)}, \quad \|\bar{\Phi}(m,n) P_n^u\| \leq K \mathrm{e}^{-\alpha_u(n-m)}.$$

Denote by

$$\mathcal{S}_J := \{x_J \in (\mathbb{R}^d)^J : \|x_J\|_\infty < \infty\}$$

the Banach space of bounded sequences indexed by J. In case $J = \mathbb{Z}$ the regularity condition (ii) in Definition (18) implies that the inhomogeneous equation

$$u_{n+1} = A_n u_n + r_n, \quad n \in \mathbb{Z}, \quad r_\mathbb{Z} \in \mathcal{S}_\mathbb{Z} \tag{57}$$

has a unique bounded solution in $\mathbb{Z}$, cf. [14, Theorem 7.6.5], [2, Theorem 4.5].

Lemma 19 *Assume that the difference equation* (56) *has an exponential dichotomy on $\mathbb{Z}$ with data $(K, \alpha_{s,u}, P_n^{s,u})$. Then*

$$\bar{u}_n := \sum_{i \in \mathbb{Z}} G(n, i+1) r_i, \ n \in \mathbb{Z}, \quad G(n,m) := \begin{cases} \Phi(n,m) P_m^s, & \text{for } n \geq m, \\ -\bar{\Phi}(n,m) P_m^u, & \text{for } n < m \end{cases} \tag{58}$$

is the unique bounded solution of (57) *on $\mathbb{Z}$.*

Note that in case $J = [n_-, n_+]$ with finite n_- or n_+, extra boundary conditions are needed to guarantee uniqueness of the solution $\bar{u}_J$.

Finally, we cite the most important perturbation result for exponential dichotomies, the Roughness Theorem, see [2, Theorem 4.4], [22, Satz 3.2.1] and [14, Theorem 7.6.7].

Theorem 20 *Assume that the difference equation* (56) *has an exponential dichotomy on* J *with data* $(K, \alpha_{s,u}, P_n^{s,u})$. *Let* $0 < \beta_{s,u} < \alpha_{s,u}$. *Then there exist positive constants* $\gamma = \gamma(K, \alpha_{s,u}, \beta_{s,u})$ *and* $\mu = \mu(K, \alpha_{s,u}, \beta_{s,u},)$, *such that for any sequence of matrices* $B_J \in (\mathbb{R}^{d,d})^J$, *satisfying* $\|B_J\|_\infty \leq \gamma$, *the perturbed equation*

$$u_{n+1} = (A_n + B_n)u_n, \quad n \in \tilde{J} \tag{59}$$

has an exponential dichotomy on J *with data* $(2K, \beta_{s,u}, Q_n^{s,u})$, *where*

$$\|P_n^s - Q_n^s\| \leq 2K\mu\|B_J\|_\infty \quad \text{for all } n \in J. \tag{60}$$

Note that explicit formulas for γ and μ may be derived from [22, Section 3] and that these constants do not depend on J.

Sketch of proof: The proof is a noninvertible version of the proof by Kleinkauf [24, Lemma 1.1.9], [23, Lemma 2.3] who followed an idea of Sandstede [36, Lemma 1.1] for continuous systems. For details, the reader is referred to [38, Satz 2.1]. For $\beta_{s,u} \in (0, \alpha_{s,u})$, introduce the exponentially weighted Banach space

$$\mathcal{Z}_J = \{X \in (\mathbb{R}^{d,d})^{J \times J} : \|X\|_* < \infty\}$$

with norm $\|X\|_* = \max\{\sup_{n \geq m} e^{\beta_s(n-m)}\|X(n,m)\|, \sup_{n < m} e^{\beta_u(m-n)}\|X(n,m)\|\}$. Consider the operators $T_1, T : \mathcal{Z}_J \times \mathcal{S}_J(\mathbb{R}^{d,d}) \to (\mathbb{R}^{d,d})^{J \times J}$ defined by

$$T_1(X, B_J)(n,m) = \sum_{l \in \tilde{J}} G(n, l+1)B_l X(l,m), \quad (n,m) \in J \times J,$$

$$T(X, B_J) = G + T_1(X, B_J),$$

where G is the Green's function of the unperturbed system from (58). A computation shows that T_1 is uniformly Lipschitz continuous in the second argument:

$$\|T_1(\cdot, B_J)\|_* \leq \mu\|B_J\|_\infty$$

with $\mu = \mu(\alpha_{s,u}, \beta_{s,u})$ independent of B_J. A crucial step is to show that $X \in \mathcal{Z}_J$ is a fixed point of $T(\cdot, B_J)$ if and only if X solves the equation

$$X(n+1, m) = (A_n + B_n)X(n,m) + \delta_{n,m-1}I, \quad n \in \tilde{J}, m \in J \tag{61}$$

subject to the boundary conditions

$$\begin{aligned} P_{n_-}^s X(n_-, m) = 0, &\quad \text{if } -\infty < n_-, \\ P_{n_+}^u X(n_+, m) = 0, &\quad \text{if } n_+ < \infty, \end{aligned} \tag{62}$$

respectively. Here, δ denotes the Kronecker symbol.

For proving this equivalence, we observe that if X is a fixed point of $T(\cdot, B_J)$, then equations (61) and (62) follows from a direct computation. For the proof of the converse statement, one studies the inhomogeneous linear equation for fixed m,

$$Y(n+1, m) - A_n Y(n,m) = B_n X(n,m) + \delta_{n,m-1}I,$$

which possesses the solution $Y = X$ by (61). Uniqueness is proven by using the dichotomy properties to show that the associated homogeneous equation possesses the trivial solution only. An application of a matrix-valued analog of Lemma 19 then yields the fixed point property.

Existence of a fixed point and thus, of a solution of (61) follows with the Banach fixed point theorem. Since $T(\cdot, B_J)$ is a uniform contraction on $\mathcal{Z}_J$ w.r.t. the norm $\|\cdot\|_*$ for sufficiently small $\|B_J\|_\infty$, we get existence and uniqueness of a fixed point $\bar{X}(B_J)$ with smooth dependence on B_J. Using the uniqueness, one shows that $Q_n^s = \bar{X}(B_J)(n,n)$ is a projector and that the perturbed equation (59) possesses an exponential dichotomy with data $(2K, \beta_{s,u}, Q_n^{s,u})$. Finally, one proves that $\bar{X}(B_J)$ is the Green's function for this system. ∎

A.2 A Lipschitz Inverse Mapping Theorem

The proof of Theorem 7 uses a quantitative version of the Lipschitz Inverse Mapping Theorem cf. [21, Appendix C].

Theorem 21 *Assume $\mathcal{Y}$ and $\mathcal{Z}$ are Banach spaces, $F \in C^1(\mathcal{Y}, \mathcal{Z})$ and let $F'(y_0)$ be a homeomorphism for some $y_0 \in \mathcal{Y}$. Let κ, η, $\delta > 0$ be three constants, such that the following estimates hold:*

$$\left\| F'(y) - F'(y_0) \right\| \leq \kappa < \eta \leq \frac{1}{\left\| F'(y_0)^{-1} \right\|} \quad \forall y \in \mathcal{B}_\delta(y_0), \tag{63}$$

$$\left\| F(y_0) \right\| \leq (\eta - \kappa)\delta. \tag{64}$$

Then F has a unique zero $\bar{y} \in \mathcal{B}_\delta(y_0)$.

References

[1] E. L. Allgower and K. Georg. *Numerical Continuation Methods.* Springer-Verlag, Berlin, 1990. An introduction.

[2] B. Aulbach and J. Kalkbrenner. Chaotic dynamics from the difference equations point of view. In *Proceedings of the First International Conference on Difference Equations (San Antonio, TX, 1994)*, pages 41–55. Gordon and Breach, Luxembourg, 1995.

[3] B. Aulbach and J. Kalkbrenner. Exponential forward splitting for noninvertible difference equations. *Comput. Math. Appl.*, 42(3-5):743–754, 2001. Advances in difference equations, III.

[4] B. Aulbach and B. Kieninger. On three definitions of chaos. *Nonlinear Dyn. Syst. Theory*, 1(1):23–37, 2001.

[5] R. Bamon, J. Kiwi, and J. Rivera. Wild Lorenz like attractors. *ArXiv*, 0508045, 2005.

[6] W.-J. Beyn and T. Hüls. Continuation and collapse of homoclinic tangles. *J. Comput. Dyn.*, 1(1):71–109, 2014.

[7] W.-J. Beyn and J.-M. Kleinkauf. Numerical approximation of homoclinic chaos. *Numer. Algorithms*, 14(1-3):25–53, 1997.

[8] V. Böhm, C. Chiarella, X.-Z. He, and T. Hüls. A homoclinic route to volatility: dynamics of asset prices under autoregressive forecasting. In *Global analysis of dynamic models in economics and finance*, pages 289–316. Springer, Heidelberg, 2013.

[9] S. Gonchenko, M.-C. Li, and M. Malkin. Generalized Hénon maps and Smale horseshoes of new types. *Int. J. Bifurcation and Chaos*, 18(10):3029–3052, 2008.

[10] S. Gonchenko, D. Turaev, and L. Šil′nikov. Homoclinic tangencies of arbitrarily high orders in conservative and dissipative two-dimensional maps. *Nonlinearity*, 20:241–275, 2007.

[11] V. S. Gonchenko, Y. A. Kuznetsov, and H. G. E. Meijer. Generalized Hénon map and bifurcations of homoclinic tangencies. *SIAM J. Appl. Dyn. Sys.*, 4:407–436, 2005.

[12] J. K. Hale and X.-B. Lin. Symbolic dynamics and nonlinear semiflows. *Ann. Mat. Pura Appl. (4)*, 144:229–259, 1986.

[13] M. Hénon. A two-dimensional mapping with a strange attractor. *Comm. Math. Phys.*, 50(1):69–77, 1976.

[14] D. Henry. *Geometric Theory of Semilinear Parabolic Equations*. Springer-Verlag, Berlin, 1981.

[15] S. Hittmeyer, B. Krauskopf, and H. M. Osinga. Interacting global invariant sets in a planar map model of wild chaos. *SIAM J. Appl. Dyn. Syst.*, 12(3):1280–1329, 2013.

[16] S. Hittmeyer, B. Krauskopf, and H. M. Osinga. From wild Lorenz-like to wild Rovella-like dynamics. Preprint, The University of Auckland, 2015.

[17] S. Hittmeyer, B. Krauskopf, and H. M. Osinga. Interactions of the Julia set with critical and (un)stable sets in an angle-doubling map on $\mathbb{C} \setminus \{0\}$. Preprint, The University of Auckland, 2015. To appear in the Internat. J. Bifur. Chaos Appl. Sci. Engrg.

[18] T. Hüls. Homoclinic orbits of non-autonomous maps and their approximation. *J. Difference Equ. Appl.*, 12(11):1103–1126, 2006.

[19] T. Hüls. Homoclinic trajectories of non-autonomous maps. *J. Difference Equ. Appl.*, 17(1):9–31, 2011.

[20] T. Hüls. A contour algorithm for computing stable fiber bundles of nonautonomous, noninvertible maps. Preprint 14060, Bielefeld University, CRC 701, 2014. To appear in SIAM J. Appl. Dyn. Sys.

[21] M. C. Irwin. *Smooth dynamical systems*, volume 17 of *Advanced Series in Nonlinear Dynamics*. World Scientific Publishing Co. Inc., River Edge, NJ, 2001. Reprint of the 1980 original, With a foreword by R. S. MacKay.

[22] J. Kalkbrenner. *Exponentielle Dichotomie und chaotische Dynamik nichtinvertierbarer Differenzengleichungen*, volume 1 of *Augsburger Mathematisch-Naturwissenschaftliche Schriften [Augsburg Mathematical-Scientific Texts]*. Dr. Bernd Wißner, Augsburg, 1994. With a foreword by Bernd Aulbach.

[23] J.-M. Kleinkauf. The numerical computation and geometrical analysis of heteroclinic tangencies. Technical Report 98-048, SFB 343, 1998.

[24] J.-M. Kleinkauf. *Numerische Analyse tangentialer homokliner Orbits*. PhD thesis, Universität Bielefeld, 1998. Shaker Verlag, Aachen.

[25] J.-M. Kleinkauf. Superconvergence estimates for the numerical computation of heteroclinics for maps. Technical Report 98-052, SFB 343, 1998.

[26] F. R. Marotto. Snap-back repellers imply chaos in $\mathbb{R}^n$. *J. Math. Anal. Appl.*, 63(1):199–223, 1978.

[27] C. Mira, L. Gardini, A. Barugola, and J.-C. Cathala. *Chaotic dynamics in two-dimensional noninvertible maps*, volume 20 of *World Scientific Series on Nonlinear Science. Series A: Monographs and Treatises*. World Scientific Publishing Co., Inc., River Edge, NJ, 1996.

[28] H. M. Osinga, B. Krauskopf, and S. Hittmeyer. Chaos and wild chaos in Lorenz-type systems. In *Theory and applications of difference equations and discrete dynamical systems*, volume 102 of *Springer Proc. Math. Stat.*, pages 75–98. Springer, Heidelberg, 2014.

[29] J. Palis and F. Takens. *Hyperbolicity and Sensitive Chaotic Dynamics at Homoclinic Bifurcations*, volume 35 of *Cambridge Studies in Advanced Mathematics*. Cambridge University Press, Cambridge, 1993.

[30] K. Palmer. *Shadowing in dynamical systems*, volume 501 of *Mathematics and its Applications*. Kluwer Academic Publishers, Dordrecht, 2000. Theory and applications.

[31] K. J. Palmer. Exponential dichotomies and transversal homoclinic points. *J. Differential Equations*, 55(2):225–256, 1984.

[32] K. J. Palmer. Exponential dichotomies, the shadowing lemma and transversal homoclinic points. In *Dynamics reported, Vol. 1*, pages 265–306. Teubner, Stuttgart, 1988.

[33] K. J. Palmer. A finite-time condition for exponential dichotomy. *J. Difference Equ. Appl.*, 17(2):221–234, 2011.

[34] S. Y. Pilyugin. *Shadowing in Dynamical Systems*, volume 1706 of *Lecture Notes in Mathematics*. Springer-Verlag, Berlin, 1999.

[35] E. Sander. Homoclinic tangles for noninvertible maps. *Nonlinear Anal.*, 41(1-2, Ser. A: Theory Methods):259–276, 2000.

[36] B. Sandstede. *Verzweigungstheorie homokliner Verdopplungen*. PhD thesis, Universität Stuttgart, 1993.

[37] B. Sandstede. Convergence estimates for the numerical approximation of homoclinic solutions. *IMA J. Numer. Anal.*, 17(3):437–462, 1997.

[38] A. Schenke. Nichtinvertierbare dynamische systeme. Master's thesis, Universität Bielefeld, 2014.

[39] L. P. Šil′nikov. On a problem of Poincaré-Birkhoff. *Mat. Sb. (N.S.)*, 74 (116):378–397, 1967.

[40] S. Smale. Differentiable dynamical systems. *Bull. Amer. Math. Soc.*, 73:747–817, 1967.

[41] H. Steinlein and H.-O. Walther. Hyperbolic sets and shadowing for noninvertible maps. In *Advanced topics in the theory of dynamical systems (Trento, 1987)*, volume 6 of *Notes Rep. Math. Sci. Engrg.*, pages 219–234. Academic Press, Boston, MA, 1989.

[42] H. Steinlein and H.-O. Walther. Hyperbolic sets, transversal homoclinic trajectories, and symbolic dynamics for C^1-maps in Banach spaces. *J. Dynam. Differential Equations*, 2(3):325–365, 1990.